ABSTRACT

Title of Dissertation: INCORPORATION OF BACTERIAL QUORUM SENSING IN SYNTHETIC BIOLOGY

Hsuan-Chen Wu, Doctor of Philosophy, 2012

Directed By: Professor William E. Bentley
Fischell Department of Bioengineering

The global objective of this research is to develop a synthetic biology toolkit consisting of molecules, cells, and devices that provide flexible, yet selective targeting, sensing, and switching capabilities, that in turn guide biological behavior in user-specified manner. We employ bacteria as “smart” programmable devices. We envision creating bacteria that autonomously move to specific areas, synthesize a drug, deliver the drug, and move on to new sites. “Targeting” endows bacterial cells the means to dock onto specific surfaces with antibody-antigen specificity. Sensing and switching capability allows bacteria to sense and, after making a “decision”, respond by synthesizing and delivering cargo to molecular scale features displayed on target surfaces. Relevant surface features may include an overexpressed receptor on a tumor cell, glucagon-like

peptide-1 receptor on pancreatic beta cells, or even other bacterial cells resident in a recalcitrant biofilm.

Towards the realization of this goal, we employed an antibody-binding protein G display strategy to complex target-binding antibodies with bacteria. We characterized the assembly and efficacy of this complex by binding to well-defined surfaces decorated with specific antigens. For sensing and switching we made use of the genetic circuitry of bacterial quorum sensing (QS) that coordinates multicellular responses. In particular, we hypothesized the creation of a biological "switch" that would take action only after a certain threshold "feature" density had been detected. Specifically, in our most significant demonstration we designed and implemented QS based sensing and actuating based on the surface density of cancer-indicating EGFR receptors displayed on epithelial cancer cell lines.

Because recent reports have demonstrated bacterial placement of a molecular "cargo" or "payload" in unrelated studies involving vaccination or direct attack on bacterial pathogens, we turned to developing innovative RNA-based drug syntheses concepts for eventual use in cancer therapy. That is, we designed RNA interfering (RNAi) technology to arrest the progression of the eukaryotic cell cycle by silencing gateway genes that serve to guide cell division and proliferation. Thus, our strategy serves to inhibit cell growth and promote cell death – actions that could find utility in treating metastatic cancer. Through a different lens, this same concept, the molecularly "programmed" manipulation of cell cycle status and cell growth via synthetic biology can

serve to promote recombinant protein production in an industrially relevant eukaryotic insect cell line.

In summary, we envision the exploitation of bacterial cells as programmable smart devices that can target, dock and deliver cargoes that are synthesized and delivered only after a set of predetermined parameters are met. We also envision a new biological "switch" that is based on the area-based density of a molecular feature – this will dramatically expand the capabilities and reach of synthetic biology. Our concepts embrace the notion that the individual cell may be the product of synthetic biology, as opposed to a synthesized molecule which is the prevailing product of choice.

INCORPORATION OF BACTERIAL QUORUM SENSING IN SYNTHETIC BIOLOGY

By

Hsuan-Chen Wu

Dissertation submitted to the Faculty of the Graduate School of the
University of Maryland, College Park, in partial fulfillment
of the requirements for the degree of
Doctor of Philosophy
2012

Advisory Committee:
Professor Williams E. Bentley, Chair
Associate Professor Adam Hsieh
Professor Peter Kofinas
Associate Professor Y. Martin Lo
Associate Professor Nam Sun Wang

Table of Contents

List of Figures

Chapter 1. Introduction

1.1. Motivation

Synthetic biology is a revolutionary field where existing biological functionality is modulated and repurposed by rewiring genetic circuits, resulting in novel biological functionality[1-5]. It focuses on the fabrication of biomolecular syntheses and cellular capacities and provides a different perspective on traditional genetic engineering. Substantial progress has been achieved in many areas of research, including biomaterials synthesis, energy production, bio-computation, and biosensors [6-16]. Additionally, more and more studies have demonstrated the potential use of synthetic biology in biomedical applications such as vaccine development, tissue engineering, and therapeutics[17-24].

Bacteria are considered one of the most important models for expediting the pace of synthetic biology progress due to their genetic accessibility. Bacterial genomes are relatively simple, well-characterized, and easy to manipulate and amplify. Besides, bacteria normally have fast growth rates, low maintenance costs, and, importantly, can produce products at high rates and yields (e.g., recombinant proteins can constitute more than 20% of the total cellular protein. This is one of the reasons bacteria are widely used in industrial fermentation and recombinant protein production processes) [25-27].

One somewhat controversial but emerging research area in synthetic biology is the use of microbes as disease or cancer fighting devices[28-30]. Historically, the potential for bacteria to serve as anticancer agents was discovered 150 years ago by German physicians, W. Busch and F. Fehleisen. They reported the regression of tumors of patients after accidental skin infections (erysipelas) caused by *Streptococcus*

pyogenes[31]. More recently, researchers have shown that tumor specific microenvironments present a preferred habitat for bacteria such as *Clostridium*, *Salmonella*, and *Escherichia* as compared to healthy tissue [32-34]. The conditions of oxygen-deprivation, chaotic vasculature, heightened metabolic byproducts, and localized inflammation associated with tumor growth that sometimes present challenges to traditional radiotherapy and chemotherapy are, in fact, ripe environments for directed anaerobic bacterial growth [35-40]. By exploiting natural bacterial capabilities, a synthetic biology approach could be used to enhance targeting specificity, tumor-killing activity, and a reduction of toxicity. In a 2010 review[41], Forbes summarized recent advances and conceptualized a model of "smart" bacteria for future therapies. He proposed an ideal "robot factory" (Figure 1-1a) that could perform important functions: target tumours, self-propel, produce cytotoxic molecules in response to triggering signals, and produce externally detectable signals. In parallel to the robot factory, bacteria (Figure 1-1b) could be engineered to carry out similar duties: steer toward chemoattractants by the control of flagella (blue), produce anticancer proteins (dark blue) in response to molecular signals (red squares), and produce detectable biomolecules (red). Through the careful tuning of bacterial phenotypes, Forbes envisioned a future of "perfect" bacteria for cancer therapies.

In part motivated by this potential, we had been pursuing parallel concepts by engineering targeting and "switching" capabilities into bacteria. Specifically, we created a targeting capability for *E. coli* by displaying *Streptococcal* antibody-binding protein G on the outer surface of *E. coli* which mediates antibody-antigen interactions on the surface of selected bacteria. In a certain sense, such a strategy iterates monoclonal

antibody blocking therapies, with an additional self-induction mechanism for further therapeutic use. The new targeting module allows bacteria to "dock" with specific surfaces of interest. Additionally, we conceived of a biological "switch" that was not envisioned by Forbes [41] in which only cells with a sufficiently up -regulated density of cancer-identifying surface receptors would be actuated upon. That is, we developed an innovative "switching" feature by leveraging the communication process of bacteria known as quorum sensing that guides multicellularity at "threshold" cell numbers. This creates a localized community based decision-making function that is autonomous, eliminating a need for intervention by external signals. Both new modules will potentially benefit the development of bacterial cancer therapies. Lastly, an RNA interference (RNAi) approach was used to arrest cell cycle progression, hindering eukaryotic cell growth, metabolically altering the cell physiology. We demonstrate by increasing recombinant protein productivity in a commercially relevant cell line. Conveniently, we have previously demonstrated that a sufficiently significant "dose" of the identical RNAi molecule (that targets cyclin E) can arrest and kill cells – revealing its potential as an anti-cancer candidate for tumor regression.

In this dissertation, we describe the component parts needed to develop this strategy. While the concepts are easily grasped, there existed few experimental approaches or platforms upon which to construct and test these concepts. We organize the dissertation in sections. We will briefly introduce the principles and technologies necessary for generating the synthetic biology modules in the latter part of Chapter one as research background. The antibody assembly strategy, which is created and tested via "biofabrication" will be discussed in Chapter two. The rewiring of bacteria for

empowering synthetic switching capability will be described in Chapter three. The metabolic engineering of eukaryotic insect cells using RNAi (payload) will be described in Chapter four. Again, this is an example for both anti-cancer therapy and bioprocess innovation. Finally, a summary and a description of future work are provided as Chapter five to merge all the elements into one functional unit.

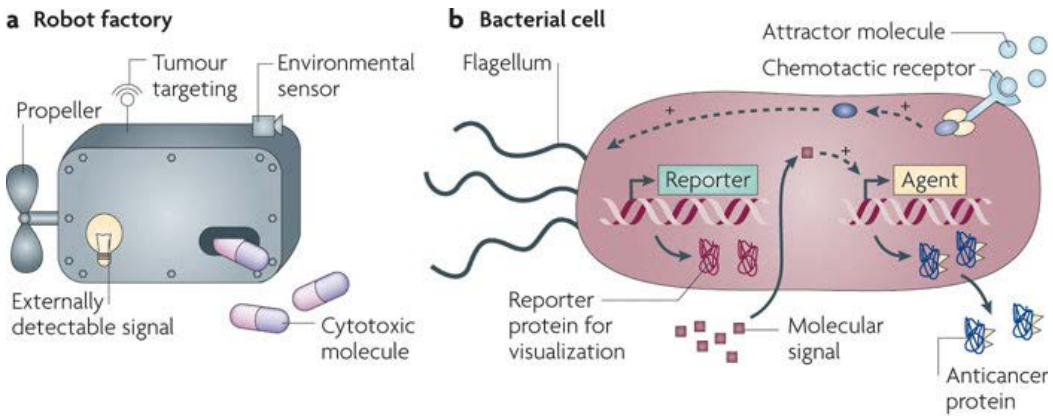

Figure 1-1 Bacteria as the optimal robot factory cancer therapies. (a) The perfect cancer therapy could be imagined as a 'robot factory' that could carry out six important functions: target tumours, produce cytotoxic molecules, self-propel, respond to triggering signals, sense the local environment and produce externally detectable signals. (b) Bacteria have biological mechanisms to carry out these functions: gene translation machinery to produce anticancer proteins (dark blue); flagella to chemotax (blue); specific gene promoter regions to respond to molecular signals (red squares); and machinery to produce detectable molecules (red). [41]

1.2. Research background – "Biofabrication" –and "Synthetic Biology"

In nature, biology employs a bottom-up means to assemble biomolecules or fabricate structures, which contrasts starkly the top-to-bottom manufacturing processes traditionally used in industry. The exploitation and repurposing of these bottom-up biological fabrication processes is defined as biofabrication. It includes the uses of cells or other biologics as the basic building blocks in which biological models, systems, devices and products are manufactured [42-44].

Synthetic biology [1-5], defined as a way to design and construct new biological parts or functions by rearranging genomes, could be considered an upstream supply line to biofabrication processes. In conjugation with biofabrication, the new biological products synthesized from synthetic biology could be fed into downstream applications. In this chapter, we combine both synthetic biology and biofabrication to create new biological switches that provide for targeting, docking, motility and payload synthesis as well as facilitate bacterial targeting by creating testing environments and assembly strategies based on biological means and components, respectively. The detailed concepts, terms, and definitions of system components are described below that when pulled together portray the potential for innovative anti-cancer therapy.

1.2.1. Biofabricated devices and assembly

Protein G is an immunoglobulin-binding protein expressed in *Streptococcal* bacteria, which selectively binds the antibody's constant (Fc) region and allows the Fab region to be active and accessible to antigens. It has been widely used in the fields of antibody purification and molecular diagnostics[45].

By repurposing protein G, we could not only orient and assemble the antibodies on a specific surface but also tether them to a supramolecular structure (i.e., the cell membrane) through biofabrication [46-48].

In Chapter two, we describe a novel antibody orientation strategy based on the covalent capture and display of protein G. This enables the hierarchical assembly of antibodies onto a specific biopolymer surface, chitosan, and facilitates the characterization of antibody assembly and antigen detection on devices and cells. That is, this protein G biofabrication method will be further exploited in Chapter three for tethering antibodies onto a bacterial outer membrane, enabling a flexible targeting functionality. This "prescribable" targeting increases the range of applications for these bacteria.

1.2.2. Enabling the switching capability: Rewiring quorum sensing circuitry for synchronizing multicellular phenotype

Quorum sensing (QS) is a microbial cell-to-cell communication process mediated through secreted signaling molecules that coordinate unicellular properties, guiding multicellular behavior [49, 50]. This is prevalent in phenotypes such as pathogenicity, biofilm formation, and virulence. In order to develop strategies against quorum sensing, its genetic regulatory structures and pathways for synthesis and signal transduction have been extensively studied with molecular resolution [51]. Recently, QS circuitry has been rewired for applications in synthetic biology, including switches, sensor devices, and recombinant protein production applications [52-54]. In this study, we linked the LuxS

quorum sensing machinery controlled by the signaling molecule autoinducer-2 (AI-2) from *E. coli* directly by creating a switching module or cassette.

A brief description of the LuxS QS circuitry follows (Figure 1-2) [54]. AI-2 based signaling is generated and processed by the *lsr* operon. AI-2 production is mediated by two enzymes: Pfs (nucleosidease) and LuxS (AI-2 synthase). First, the precursor S-adenosylhomomcycteine (SAH), which is the intermediate metabolite from biosynthesis or modification of DNA, RNA and proteins, is converted to S-ribosylhomocysteine (SRH) by Pfs. SRH is then catalyzed into 4,5-dihydroxy-2,3-pentanedione(DPD) by LuxS. The resulting DPD is spontaneously cyclized into the signaling molecule AI-2. Initially, AI-2 accumulates extracellularly during the low density phase of bacterial growth (early growth phase). Thereafter, AI-2 is imported back into cells by the Lsr ABC-type transporter when cell density reaches a putative threshold (near early stationary phase). Intracellular AI-2 is then phosphorylated by LsrK kinase and the resultant phospho-AI-2 activates further expression of Lsr components by binding and releasing LsrR (the repressor of the *lsr* operon) from the DNA. This combined negative and positive feedback of AI-2 mediated QS results in the tight regulation of the multicellular switch. By harnessing and further amplifying the QS switch-like signal, the bacteria can decide whether or not to turn on gene expression “smartly” by evaluating the “feature” density in local environments. Further details will be described in Chapter three.

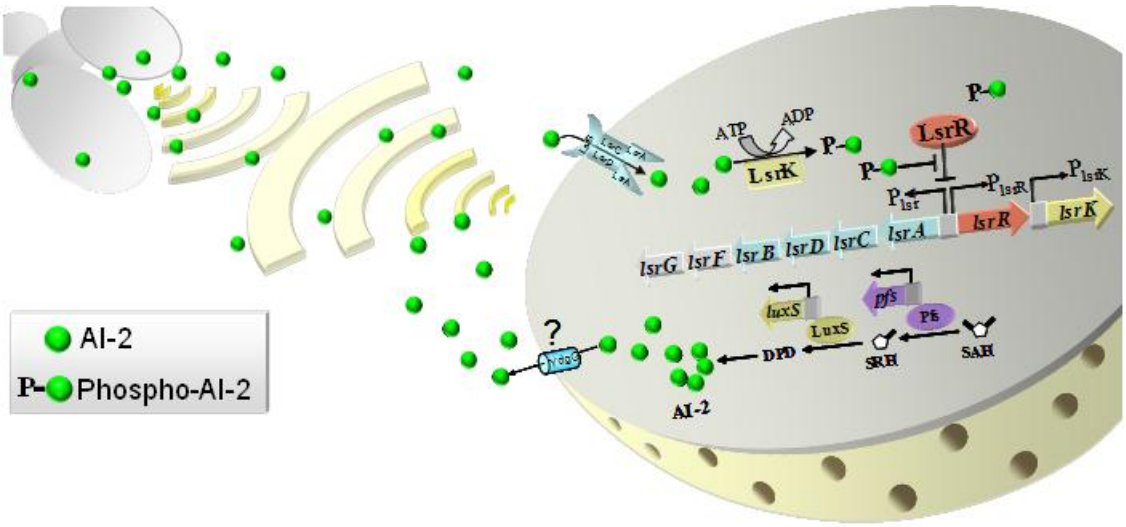

Figure 1-2 AI-2 mediated QS communication. The signal generation, uptake, and derepression of *lsr* operon in *E. coli*. AI-2 (green sphere) is produced from S-adenosylhomocysteine (SAH) by Pfs and LuxS and accumulates extracellularly with low cell density. AI-2 is internalized by the Lsr transporter followed by phosphorylation via kinase, LsrK. Phospho-AI-2 (green sphere-P) de-represses both the *lsr* and *lsrRK* promoters. [54]

1.2.3. Eukaryotic insect cell cycle and proliferation control using RNAi : Cell cycle arrest as an anti-cancer strategy

1.2.3.1. Cell cycle

The eukaryotic cell cycle consists of both the machinery that governs cell division in all its stepwise facets and the cell division itself. As such, it plays a crucial role in embryonic development and differentiation, cell death or apoptosis, DNA repair, angiogenesis, and tumorigenesis [55-62]. Researchers have also found that that cell cycle and cell proliferation status are closely related to the activity of protein synthesis machinery [63] and as such, have targeted the cell cycle as a tool for altering the metabolic landscape for product synthesis. As indicated in Figure 1-3, the cell cycle can be divided into four distinct phases: G1 phase, S phase, G2 phase and M phase (mitosis). S and M phases represent DNA synthesis and mitosis phases respectively, and phases in

between are G1 (“gap-1”) and G2 (“gap-2”) phases. Not only acting as “gaps”, the biosynthetic activities of proteins and enzymes are highly active in G1 and G2 phases [64], which are also termed “growth” phases.

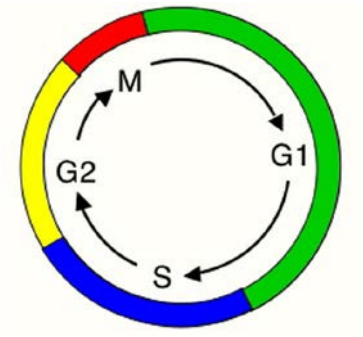

Figure 1-3 Simple representations of the cell cycle. A typical (somatic) cell cycle can be divided into four sequential phases: G1 (gap-1), S (DNA replication), G2 (gap-1), and M (mitosis). [58]

1.2.3.2. RNAi

RNA interference (RNAi) is a cellular process that inhibits gene expression by degrading specific RNA species resulting in selective gene silencing. RNAi was initially found in plants as a means for viral defense. The use of antisense RNA to interfere with gene activity in *C. elegans* was first utilized by Guo and Kemphues (1995) to study par-1 function [65]. Subsequently dsRNA, formed by the annealing of sense and anti-sense strands, was discovered and used by Fire et al. 1998 [66], who subsequently won the Nobel prize. As presented in Figure 1-4, dsRNA mediated gene silencing results from the cleavage of long dsRNA by Dicer (RNAse III) into 21-25 small interfering RNA (siRNA). These siRNAs then associate with RNA-induced silencing complex (RISC) through which they are processed to become single-stranded RNA that guide the RISC

complex to target mRNA. Degradation and silencing of specific mRNA species is the consequence. Due to this ability to knockdown or silence gene expression, RNAi has become a common and convenient tool in studies of gene function and has been widely used in developmental biology [67], medicine [68], functional proteomics[69-71] as well as metabolic engineering [72, 73]

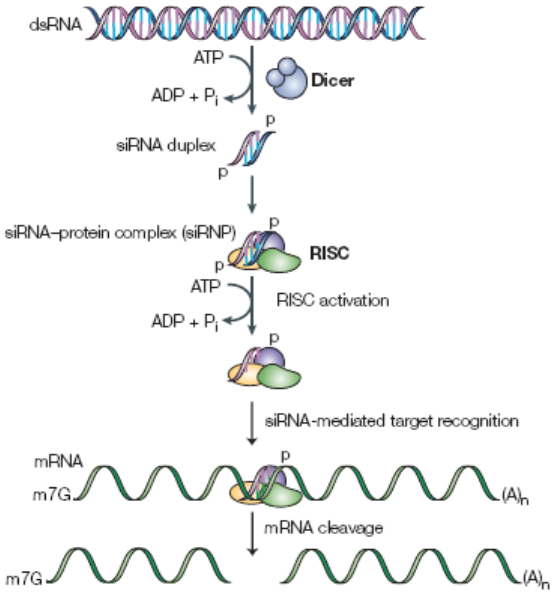

Figure 1-4 RNA interference pathway. dsRNA is cleaved into siRNAs by dicer and the resultant siRNAs associate with RISC. Unwinding of siRNA results in target mRNA recognition and subsequent gene silencing by RISC cleavage. [74]

In Chapter four, RNAi is used to silence a novel insect cell line homologue of the positive cell cycle G1 regulator, Cyclin E. This knockdown resulted in cell cycle arrest at the G1 phase, decreasing cell growth and enhancing recombinant production synthesis, a useful outcome from a metabolic engineering perspective.

This result also concerns cancer biology, since defective cell cycle regulation is a common attribute of oncogenic phenotypes [75]. As previously described, the cell cycle

consists of important machinery for cell division and proliferation in eukaryotic cells, ensuring daughter cell integrity and survivability. Cancer cells that have escaped from the cell cycle reproduce abnormal cells rapidly and form tumors due to unchecked growth. Re-activation of cell cycle regulation by arresting the cancer cells using RNAi is therefore a plausible target for cancer therapy.

Chapter 2. Biofabrication of antibodies and antigens via IgG-binding domain engineered with activatable pentatyrosine pro-tag

2.1. Introduction

Antibodies are biological recognition elements extensively used for laboratory-based immunoanalysis [76-78]. Antibodies are also integral to immuno-affinity-chromatography for the purification and separation of proteins [79, 80]. Efforts to extend the use of antibodies within sensors and devices have attempted to ensure the proper orientation of their antigen-binding sites [81-86]. That is, it is well recognized that the various antibody assembly techniques can lead to reduced antigen binding capacity (via steric hindrance, denaturation, chemical modification [48, 87]. In nature, antibodies can be oriented, for example, at cell surfaces by binding to membrane-bound proteins that selectively bind the antibody's constant (Fc) region. Not only do these binding proteins orient the antibodies, but they also tether them to a supramolecular structure (i.e., the cell membrane). Using lessons from nature, we employ three biologically-based methods for the hierarchical assembly of antibodies into macroscopic systems [46].

Specifically, in this work, we make use of immunoglobulin (Ig) binding proteins derived from the cell surfaces of bacteria. These proteins selectively bind the antibody's constant (Fc) region and free the antigen-binding (Fab) site to interact with antigens [48, 88-90]. We have genetically modified a *Streptococcal* IgG binding domain (derived from protein G) to serve as a scaffold for the generic assembly of antibodies onto a variety of surfaces. Namely, we have incorporated a tyrosine rich ''pro-tag'' at the C-terminus of protein G [91, 92]. These tyrosyl residues are enzymatically activated by

tyrosinase to quinones, which then covalently couple to the primary amines of pH-stimuli responsive polysaccharide chitosan [93-96].

Our approach, outlined in Figure 2-1, builds upon nature's methods to orient antibodies onto supramolecular structures. Self-assembly is employed to bind antibodies to the engineered protein G. As noted, Protein G was engineered for enzymatic-assembly by genetically fusing a C-terminal $(tyr)_5$ pro-tag that can be selectively activated by tyrosinase for covalent conjugation to the aminopolysaccharide chitosan. Assembly from the nano- to the macro-scale is achieved by the directed-assembly of chitosan in response to external stimuli[97]. Central to this ‘‘biofabrication’’ approach are: (1) the pH dependent solubility characteristics of chitosan, shown previously to enable pH-based ‘‘switching’’ of the solubility of a chitosan-conjugated protein, and (2) the enzymatic activation of a protein G Fc-binding domain shown here for the first time.

Of note, the protein G used in this study was originally engineered to be a fusion with three repeats of the antibodybinding domain and 72 repeats of the pentapeptide derived from the hydrophobic domain of elastin (designated E72G3) [47]. Protein G fusions with elastin adhere non-covalently to hydrophobic surfaces [47, 98]. We modified E72G3 by deleting the elastin repeats, adding a pentatyrosine sequence to the C-terminus, and expressing the protein from a plasmid within *E. coli* that adds an N-terminal histidine tag to yield the protein HG3T [99]. This facilitates coupling of protein G to chitosan, and further, assembly of the protein G, antibodies, and antigens into three model device formats (96-well microtiter plates, microfabricated chips, and a fiber mesh).

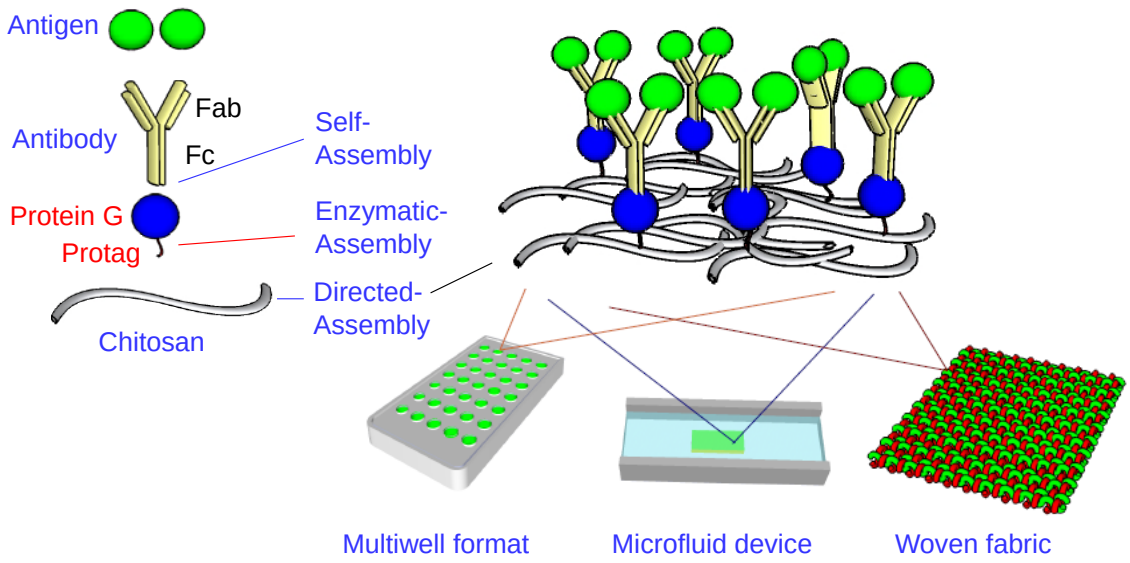

Figure 2-1 Schematic of three biofabrication methods used for hierarchical assembly (not to scale). At the nanoscale, antibody binds to the Streptococcal protein G while the protag fused to protein G allows its enzyme-mediated conjugation to the aminopolysaccharide chitosan. The stimuli-responsive network-forming properties of chitosan allow assembly at the micro- and macro-scales. Hierarchical assembly is suggested for three formats; conventional multiwell plates, electrode addresses within microfluidic channels, and fibers for woven fabrics.

2.2. Materials and methods

Antigens and Antibodies

Two fluorescent antigens were used in this study, Texas-red labeled bovine serum albumin (BSA; Invitrogen) and green fluorescent protein (GFP). GFP was expressed from *E. coli* BL21 and purified using standard methods [100]. Five alkaline-phosphatase-linked antibodies were used in this study; goat anti-guinea pig (Kirkegaard and Perry Laboratories), goat anti-mouse (Sigma), goat anti-rabbit (Sigma), rabbit anti-chicken (Sigma) and rabbit anti-goat (Sigma). Two fluorescently-labeled antibodies were used; FITC-labeled goat anti-mouse (Sigma) and Texas red-labeled goat anti-rabbit (Rockland Immunochemicals). Two antibodies were used to study antigen binding, goat anti-GFP (Rockland Immunochemicals) and goat anti-BSA (Sigma).

Vector Construction and Fusion Protein (HG3T) Expression

As partially described in Shi et al. 2008, we PCR-amplified the 3 repeats of the Streptococcus protein G Fc-binding domain (designated as G3) from the template vector pET32-E72G3 which, in turn, has the G3 domain fused to 72 repeats of the pentapeptide (E72) from the hydrophobic domain of elastin [47]. PCR primers within the reaction contained an extra sequence at the 3' end that codes for the pentatyrosine protag (designated as T). The resulting PCR product (G3T) was ligated into a blunt II-TOPO vector and then transformed into TOP10 *E. coli* cells for pTOPO-G3T amplification. The G3T DNA fragment excised from pTOPO-G3T by EcoRI and NcoI was inserted into a pET32 vector that codes for an N-terminal histidine tag. The protein product expressed from the pET32-G3T plasmid is designated HG3T. The pET32-HG3T vector was transformed into *E. coli* BL21(DE3) for protein expression. The cells were inoculated into LB medium with ampicillin (100 μg/ml) and grown 16 hours at 37^{o}C and 250 rpm

shaking. These cells were transferred into fresh LB media (1% inoculation ratio), grown to an OD_{600} of 0.5, and induced by adding IPTG (1 mM final concentration). The induced cell culture was transferred to a 30^{o}C w/ shaking environment and incubated for 4-6 hours. The cells were then collected by centrifugation and lysed using Bugbuster reagent (Novagen). The supernatant was separated from cell debris by centrifugation and recombinant proteins were purified by Talon metal affinity resins (Clontech). The final HG3T product was desalted by dialysis.

Protein Analysis using LabChip

Cell extracts and purified HG3T proteins were analyzed using 2100 Bioanalyzer (Agilent Technologies). First, the protein samples were mixed with the denaturing solution (Agilent Protein 230 Kit) and heated for five minutes. After cooling, samples were loaded into the pre-cast protein chip. Molecular weights of each major component in the cell lysate and HG3T samples were determined by the Bioanalyzer. Bovine serum albumin (BSA, New England Biolabs) with M.W. ~66.43KDa was used as a control.

Western Blots

Protein HG3T was mixed with sampling buffer and then heated to 95^{o}C for ten minutes. Samples were then loaded into multiple wells and run on a 12.5% SDS-PAGE gel at 150 volts for 1 hour. Protein was then transferred to nitrocellulose membranes by a BioRad Trans-Blot semi-dry transfer cell with BSN transfer buffer (48 mM Tris, 39 mM glycine, 20% v/v methanol, 0.0375% w/v SDS) and a voltage of 15 volts for 20 minutes and then 20 volts for 20 minutes. The nitrocellulose membrane was then washed 3 times

with TBS (20mM Tris-HCl, pH 7.5, 500 mM NaCl), blocked with 5% (w/v) nonfat dry milk in TBS for two hours, and washed 3 times with Tween-containing TBS (0.05% v/v Tween 20). The nitrocellulose membranes containing HG3T were then cut into pieces and incubated for 1 hour with different enzyme-linked antibodies that had been diluted in TBS buffer containing Tween 20 (0.05 %) and nonfat dry milk (1 %). The antibodies were from 2 separate hosts (rabbit and goat) and were linked with alkaline phosphatase (AP). After washing the membrane pieces 3 times with Tween-containing TBS and then TBS, the membranes were developed by adding the indolyl phosphate substrate solution and incubating for several minutes. The substrate solution was prepared by diluting commercially-available NBT/BCIP substrate (Roche) with Tris-HCl buffer (0.1 M, pH 9.5) containing NaCl (0.1 M,) and $MgCl_2$ (0.05 M).

Tyrosinase Activation of HG3T and Conjugation to Chitosan

Various amount of protein HG3T was added in wells of 96 well plate and each was mixed with tyrosinase (350U). 100 nmoles of *o*-phenylenediamine (OPD; Sigma) was added in each of the reacting well to final volume of each well 200 ul. The positive control using catechol (Sigma) was conducted with equivalent amount to protein HG3T. Absorbance of the reaction product was detected by plate reader at the wavelength of 450nm. For chitosan conjugation studies, chitosan films were first cast on the bottom of each well of a 96-well plate by pipetting a chitosan solution (0.5 w/v % pH 4.8) into the well, drying overnight at 45 °C, neutralizing with NaOH (1 M) for 30 minutes, and washing three times with 0.01 M PBS. The reactions were performed in the chitosan-casted wells by the combination of HG3T (0.72 nmoles), E72G3 (0.72 nmoles), and

tyrosinase (350 units) to final volume of 200 ul. The solutions were incubated for 2 hours and after which the solutions were pipetted into a cuvette and the UV-Vis spectrum was measured.

Multiwell plate studies

Enzymatic assembly of protein HG3T was performed by adding tyrosinase (100 U/ml) and the (tyr)5-tagged protein G (HG3T) to each chitosan-coated well (the amount of HG3T was varied) and incubating overnight at room temperature in an orbital shaker. After enzymatic assembly, the wells were rinsed three times with PBS and incubated with NaBH4 (0.2% w/v in PBS) for 15 minutes. After assembling HG3T, the plate was washed three times with PBS, incubated for 2 hours with a blocking solution (5 % w/v nonfat milk in 0.01 M PBS), and rinsed three times with tween-containing PBS (TPBS; 0.05% v/v Tween 20 in PBS). Antibodies were then and diluted in TPBS containing 1% nonfat milk. Antibodies were assembled in each well by adding the diluted antibody solutions and incubating for 1 hour. After antibody assembly, the plate was washed three times with TPBS and then rinsed with PBS. When alkaline-phosphatase (AP) linked antibody was studied, the wells were first rinsed with a solution containing diethanolamine (DEA; 0.1 M), and then incubated for 30 minutes with the substrate solution containing p-nitrophenylphosphate (pNPP; 0.1% w/v) plus DEA (0.1 M). For antigen-binding studies, the GFP antigen was diluted in PBS and incubated for one hour in wells containing the anti-GFP antibody (goat anti-GFP) after which the wells were washed three times with TPBS. Plate readers were used to measure either absorbance or fluorescence in studies with 96-well plates. Absorbance was used to measure products

generated from reactions of the AP-linked antibody (405 nm). Fluorescence was used to measure binding of FITC-labeled antibodies (excitation filter 494 nm, emission 521nm) and GFP (excitation filter 395 nm, emission 509 nm).

Chip studies

Chitosan was electrodeposited onto the left electrode by partially immersing the chip in a chitosan solution (0.8 w/v %, pH 5.5) and applying a negative voltage to left lead. Deposition was performed for 1 minute at a constant current density of 3 A/m^2 (typically the applied voltage was 2-3 volts). After deposition, the chips were disconnected from the power supply, removed from the deposition bath, and rinsed with water and then twice with PBS buffer (pH 7.4). HG3T was enzymatically-assembled to the electrodeposited chitosan film by incubating the chip overnight in 2 ml solution containing tyrosinase (100 U/ml) and HG3T (0.8 uM), after which it was incubated for 15 minutes with NaBH4 (0.2% w/v in PBS). After HG3T assembly, the chips were rinsed, immersed in a milk blocking solution (5 % nonfat milk in PBS) for 2 hours and then rinsed three times with TPBS. Antibody was then assembled by incubating the chip for 1 hour in 2 ml of anti-GFP antibody solutions (0.3 uM diluted in 1% milk TPBS solution). Antigen binding was then achieved by immersing the chip in a 2 ml solution containing the GFP antigen and incubating for 1 hour after which the chips were washed with PBS. Fluorescence images of chips were obtained with a Leica fluorescence microscope using the following filter sets; FITC-labeled antibody (excitation 480/40 nm, emission 510 nm), GFP (excitation 425/60 nm, emission 480 nm), and Texas-red-labeled BSA (excitation

560/55 nm, emission 645/75 nm). Fluorescence photomicrographs were then analyzed using ImageJ software (National Institutes of Health).

Fiber studies

Chitosan fibers were prepared by injecting a chitosan solution (1.6 w/v %, pH = 5.0) through a 27 gauge needle into an aqueous solution containing 20 % ethanol and 1 M NaOH, and allowing the fibers to incubate in this bath for 10 minutes. The resulting fibers were rinsed with PBS, and the HG3T protein was assembled by contacting the fibers overnight with a solution of HG3T (0.8 uM) and tyrosinase (100 U/ml), and then incubating the fibers for 15 minutes with NaBH4 (0.2% w/v in PBS). After enzymatic assembly of HG3T, the fibers were blocked (5 % nonfat milk in PBS). For antibody assembly, the HG3T-conjugated fibers were incubated for 1 hour with 2 ml of either anti-GFP antibody (0.3 uM) or anti-BSA antibody (0.1 uM). In initial experiments, the anti-GFP fibers were incubated for 1 hour with the GFP antigen (0.17 uM). In later studies, a loose fiber mesh was created from both the anti-GFP presenting and the anti-BSA presenting fibers, and this mesh was incubated for 1 hour with an antigen mixture containing GFP (0.17 uM) and Texas-red-labeled BSA (0.08 uM). Fluorescence images of fibers were measured using the sample procedures as described above in chips studies.

2.3. Results and discussion

Expression and Characterization of HG3T Scaffold

Figure 2-2a depicts the resultant expression sequences within pET32-HG3T for HG3T synthesis in *E. coli*. In Figure 2-2b**,** the estimated M.W. of BSA is ~66KDa which is consistent with its known molecular weight. The purified protein migrates within the SDS-PAGE at ~43KDa, also consistent with its predicted value (~40 KDa). Immunoblots for antibody capture (Figure 2-2c**)** indicate that the engineered protein G (HG3T) can bind many different antibodies derived from both rabbit and goat. Hence, the HG3T scaffold is of general utility for the assembly of antibodies. We note the protein G used in this study (HG3T) was originally engineered as a fusion with three repeats of the antibody-binding domain and 72 repeats of the pentapeptide derived from the hydrophobic domain of elastin (designated E72G3). In experiments not shown, we added HG3T, E72G3, and GFP (control) to individual wells, performed SDS-PAGE and Western blots using alkaline phosphatase-linked antibody (anti-goat). We found comparable binding of antibody to HG3T and E72G3 (and none to the GFP control). Hence, we believe the C-terminal pentatyrosine fusion tag does not adversely affect antibody binding to the HG3T protein.

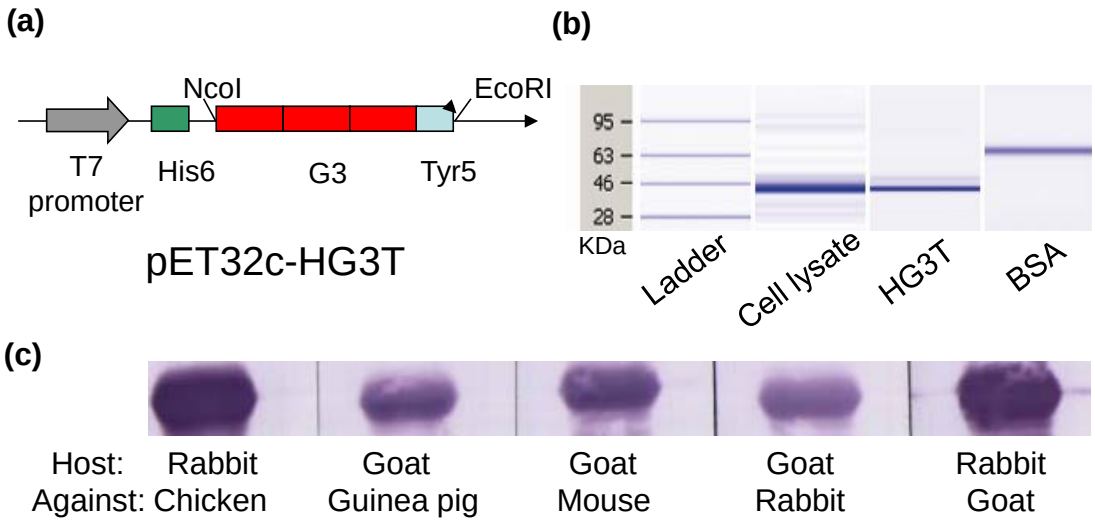

Figure 2-2 Protein G (HG3T) expression and activity characterization. (a) Vector pET32-HG3T was constructed by deleting elastin domain and adding pentatyrosine tag (Tyr5) from the original pET32-E72G3 vector. (b) SDS-PAGE result of purified protein HG3T indicating molecular weight ~43KDa comparable to the theoretical M.W. ~40KDa. (c) Antibody binding activity of HG3T was shown in western blots using various antibodies as indicated.

Activation of the engineered protein G (HG3T) by tyrosinase was investigated for the first time using *o*-phenylenediamine (OPD). Chemical analysis of the pentatyrosine tag activation was not shown previously [101], its use here suggests single residue activation by tyrosinase. As illustrated in Figure 2-3a, OPD reacts with *o*-quinones to generate a phenazine complex that absorbs at 450 nm[102, 103]. When HG3T is incubated with tyrosinase and OPD, there is a large increase in absorbance as shown in Figure 2-3b. Controls lacking tyrosinase or HG3T (i.e., the y-intercept in Figure 2-3b) show no absorbance increases, while the control lacking OPD shows small absorbance increases consistent with tyrosinase-mediated browning reactions. These results indicate that tyrosinase activates HG3T by converting tyrosine residues into reactive *o*-quinone residues. To provide a preliminary estimate of the number of tyrosine residues activated by tyrosinase, we incubated the small-molecule chemically-active analogue, catechol,

with tyrosinase and OPD, and measured the absorbance increase. Catechol was incubated with OPD and tyrosinase at the identical molar concentration as HG3T. Catechol, which contains a singular reactive site and resultant *o*-quinone, was observed to absorb 450 nm light nearly identically to HG3T as a function of OPD concentration (Figure 2-3b). The nearly identical slopes in these curves along with similar absolute absorbance suggest that the functional dependence of the reaction with OPD is the same between the two reactions. Because there is one reactive site within catechol, these results support the notion that tyrosinase oxidizes one tyrosine residue per HG3T protein. We further note there was no absorbance increase when the E72G3 protein (no tyrosine tag) was incubated with tyrosinase and OPD.

In our previous work introducing the tyrosine pro-tag concept [92, 93], we demonstrated the coupling of GFP to chitosan. Additionally, two bacterial enzymes, Pfs and LuxS, have been enzymatically conjugated to chitosan [104, 105]. Evidence that the tyrosinase-activated HG3T protein can be conjugated to chitosan is provided in Figure 2-3c. In this experiment, cast chitosan films were incubated with tyrosinase and HG3T, and these films were observed to have large increases in absorbance at wavelengths above 350 nm. Control films incubated without tyrosinase or HG3T show little absorbance above 350 nm, and films incubated with the E72G3 protein plus tyrosinase also show no absorbance above 350 nm. Increased UV-Vis (300nm-700nm) absorbance provides evidence for quinone-mediated reactions [101, 106]. The results in Figure 2-3c are consistent with those in Figure 2-3b and indicate that tyrosinase can selectively activate the protag for assembly of the HG3T protein onto chitosan.

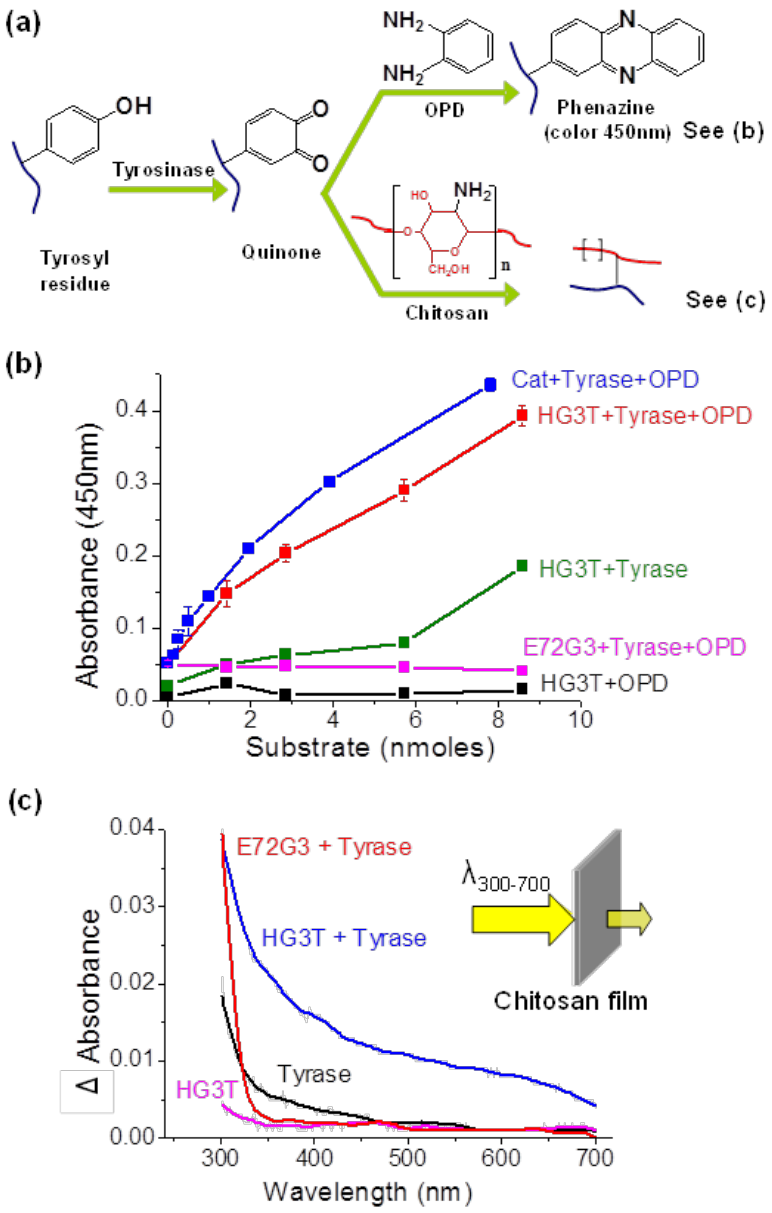

Figure 2-3 Enzymatic activation of $(tyr)_5$-tagged protein G (HG3T) and conjugation to chitosan. (a) The reaction schematic of the tyrosinase activation of HG3T and conjugation to chitosan. (b) Tyrosinase-mediated activation is observed using OPD to generate the phenazine chromophore. Similarities in the curves for the experimental samples (HG3T + Tyrase + OPD) and controls using the small molecule analogue catechol (Cat) suggest one tyrosine residue is activated per HG3T protein. The failure of tyrosinase to activate E72G3 indicates that activation requires the tyrosine residues of the protag. (c) Conjugation of the HG3T protein to chitosan was studied by incubating chitosan films with components and measuring the absorbance increase of the film. Absorbance above 350 nm indicates the tyrosinase-mediated conjugation of HG3T to the chitosan film.

Biofabrication of Antibody/Antigen Assemblies

The methods described in the next sections demonstrate biological means to fabricate biomolecular complexes that preserve biological function of their component parts. We have refered to this process as “biofabrication” [46].

Multiwell plate format

To test the function of the protein G-mediated assembly of antibodies, we fabricated the equivalent of an ELISA. Chitosan films were cast on the bottom of each well, HG3T was enzymatically-assembled onto these films using tyrosinase, antibody was allowed to self-assemble to this surface-bound protein G by incubation for 2 hours. In our first study, we used an alkaline phosphatase-linked antibody (rabbit anti-goat) and measured antibody binding by incubating with the AP-substrate. As shown in Figure 2-4a, the absorbance associated with the AP-reaction increases monotonically with HG3T. Considerably less absorbance is observed for the control in which tyrosinase was deleted from the HG3T assembly step. Antibody binding to the assembled HG3T was confirmed in a second multiwell plate experiment using fluorescently-labeled antibody (FITC-labeled goat anti-mouse antibody). Figure 2-4b shows increased fluorescence intensity with increasing concentration of HG3T. A final study using the multiwell plate format was performed to demonstrate that the assembled antibody retains antigen-binding ability. Specifically, we generated an antibody-HG3T-chitosan assembly using antibody for the green fluorescent protein (goat anti-GFP antibody). Figure 2-4c shows saturation behavior for binding of the antigen GFP to this assembly. The results in Fig 2-4 confirm

that HG3T that is conjugated to chitosan can quantitatively assemble antibodies that can subsequently bind antigens.

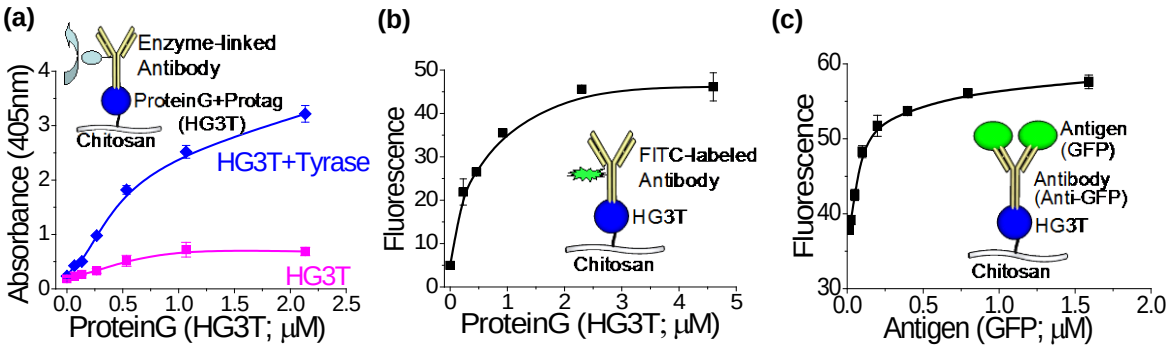

Figure 2-4 Antibody assembly and antigen binding using conventional 96-well plates with cast chitosan and HG3T assembled in each well. Antibody assembly was confirmed using; (a) alkaline phosphatase-linked rabbit anti-goat antibody (0.4 uM) with the pNPP substrate, and (b) FITC-labeled goat anti-mouse antibody (2 uM). (c) Antigen binding was confirmed using goat anti-GFP antibody (1.2 uM) and the GFP antigen.

Electrodeposited Chitosan

Chitosan's pH-responsive network-forming properties offer unique opportunities for extending antibody-based analysis from conventional multiwell plate formats to lab-on-a-chip devices[46]. Chitosan can be induced to undergo a localized sol-gel transition in response to a pH gradient established at a cathode surface[107-109]. After rinsing, an electrodeposited chitosan film is stable in the absence of an applied voltage where the pH is retained above about 6.5 (chitosan re-dissolves at low pH). Properties of the electrodeposited chitosan (e.g. thin film, matrix, or hydrogel) depend on the deposition characteristics [110]. To test whether electrodeposited spatially-resolved chitosan films allow antibody assembly we used the chips shown in Figure 2-5a. Chitosan was electrodeposited onto the left electrodes of these chips and then HG3T was enzymatically-assembled onto the electrodeposited chitosan (e.g. Figure 2-4). Next, the chips were incubated with a fluorescently-labeled antibody (FITC-labeled goat anti-

mouse antibody). Figure 2-5a depicts the loading of antibody onto the chitosan varies with the concentration of antibody in the incubation mixture. There was a linear relationhip between the electrode's fluorescence and the antibody concentration. These results demonstrate that chitosan's electrodeposition retains its reactivity for tyrosinase-mediated conjugation and antibodies can be quantitatively assembled using the protein G scaffold.

To test antigen assembly onto the antibodies, we electrodeposited chitosan, enzymatically-assembled HG3T to the left electrodes (Fig 2-5b), and then assembled an anti-GFP antibody. Chips were then incubated with various amounts of GFP antigen. The fluorescence images show GFP is assembled onto the left electrode with high spatial selectivity, while the plot shows a semi-quantitative relationship between electrode's fluorescence and antigen levels in the incubation solution. In summary, the results in Figure 2-5 illustrate that the biologically-based assembly methods provide a simple and generic means to assemble antibodies (and antigens) at specific electrode addresses and that the protein G scaffold apparently had negligible interference with the assembly of antigens onto the assembled antibodies.

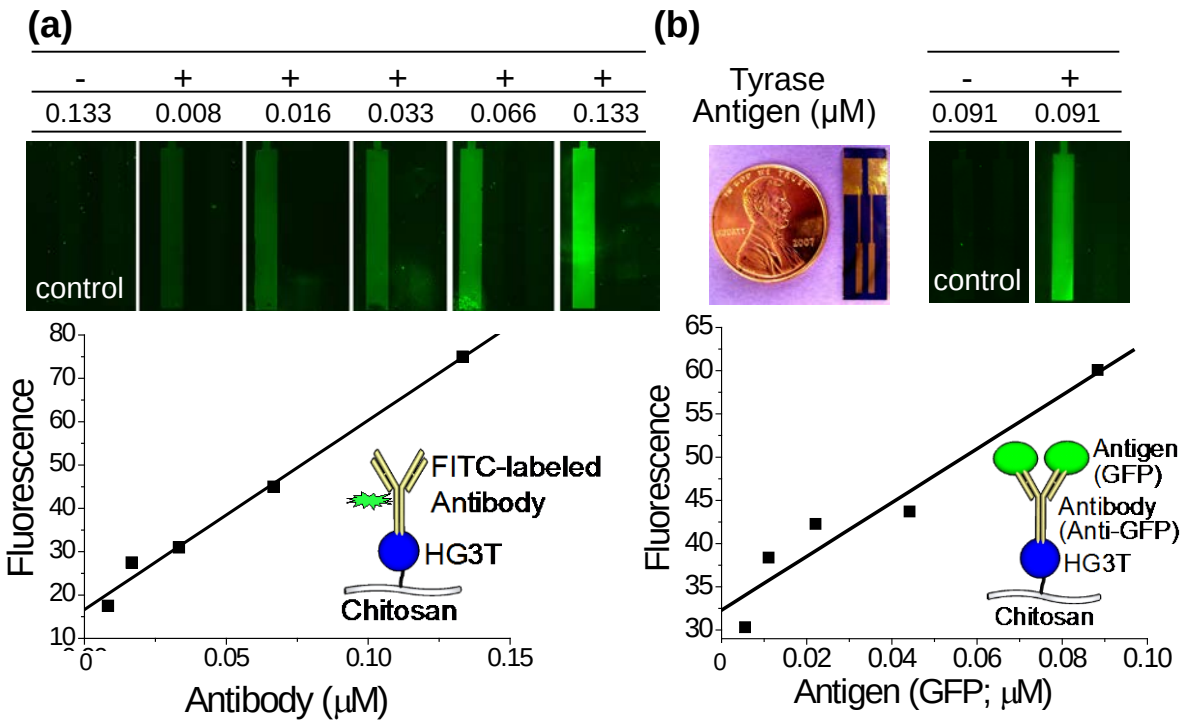

Figure 2-5 Spatially-selective antibody assembly and antigen binding at electrode addresses of a patterned chip. (a) Antibody was assembled by the following sequence: directed-assembly of chitosan by electrodeposition on the left electrodes; enzymatic-assembly of the HG3T onto the electrodeposited chitosan; and self-assembly of FITC-labeled anti-mouse antibody by binding to HG3T. Fluorescence images and image analysis indicate spatially-selective and quantitative antibody assembly at the electrode addresses (R^2=0.995). (b) Antigen binding was studied by assembling goat anti-GFP antibody onto the left electrodes and incubating the chips with varying concentrations of the GFP antigen (R^2=0.962). Note: the right electrodes serve as controls that lack chitosan.

"Smart" Fibers

Chitosan's pH-responsive, network-forming properties also allow fibers to be spun or electrospun [111-113]. Chitosan fibers (Figure 2-6a) were prepared by injecting a chitosan solution into an ethanolic alkaline bath. The fiber diameter was approximately 500 um. An initial study was performed to assemble two antibodies at separate locations on a single fiber. This was achieved by simultaneously immersing each end of the fiber

into separate antibody solutions; a goat anti-rabbit antibody labeled with Texas red (0.1 uM) and a goat anti-mouse antibody labeled with FITC (0.1 uM). The fluorescence image shows assembly of the labeled antibodies at separate "addresses" on the fiber while no fluorescence is observed in the middle of the fiber where no antibody was assembled.

Assembly of antigen was similarly tested. Freshly extruded fibers were sequentially incubated with tyrosinase plus HG3T, anti-GFP antibody, and then dipped into solutions containing GFP. The fluorescence photographs and associated image analyses indicate considerable GFP binding (Figure 2-6b**)**. In contrast, the control fiber on the left (tyrosinase was deleted during the HG3T assembly step) shows little fluorescence (both in the image and by image analysis). Thus, antibody-presenting chitosan fibers can be readily generated for antigen capture.

In studies analogous to the electrodeposited chitosan, we tested the extent to which the antibody and antigens could be assembled onto fibers. While our results are promising, error due to the nonuniformity in fiber geometry (thickness or cross sectional area varies along fiber length), the antigen loading was difficult to quantify using image analysis. To circumvent this difficulty, we dissolved individual fibers assembled with GFP using mild acid (0.1 M acetate buffer, pH 5.0) and measured the fluorescence in solution. The relationship depicted in Figure 2-6c is indeed linear (R^2=0.993), illustrating quantitative assembly of antibody and antigen onto chitosan fibers. Indeed, the slope of Fig 2-6c also enables an estimate for the number density of GFP on the surface of fiber. That is, our results suggest that 5 pmole of the GFP antigen is bound per cm of the antibody-presenting chitosan fiber (diameter ≈ 0.5 mm). If the average cross-sectional

area of GFP is estimated to be 8 nm^2/molecule, then a "fractional" surface coverage of antigen on the fiber (area occupied by protein/fiber area) is on the order of 2. This estimate suggests that antigen-antibody binding is not confined to the external surface of the chitosan fiber but, instead, suggests that some binding occurs within the fiber network. Analogous observations were made for antigen-antibody binding within agarose networks [114] and for nucleic acid hybridization within chitosan films [115].

The ability to generate antibody-presenting fibers also suggests the potential for creating woven fabrics with the ability to capture multiple antigens simultaneously. We generated chitosan fibers with two different antibodies – one against GFP and a second against bovine serum albumin (BSA) – and we created a loose mesh of these two types of fibers. This mesh was then immersed in a solution containing a mixture of both the GFP and BSA antigens (BSA was fluorescently labeled for imaging). Fig 2-6d shows fluorescence images for this mesh and indicates that each antigen is assembled on its respective fiber. These results indicate that woven fabrics can be prepared to capture multiple antigens simultaneously.

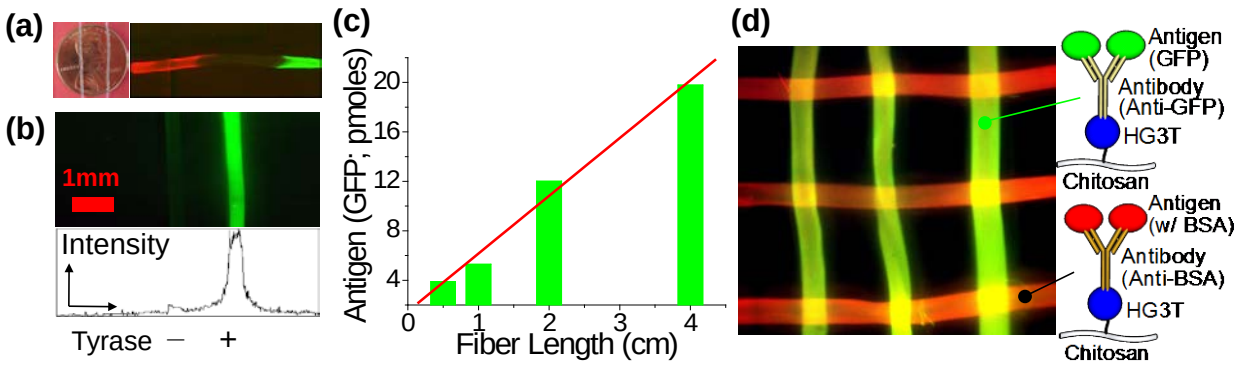

Figure 2-6 Antigen binding to antibody-presenting chitosan fibers. (a) Optical micrographs provide a perspective of the fiber size (~500 um diameter in this case). The versatility of antibody assembly onto chitosan fibers is illustrated by the assembly of two different fluorescently-labeled antibodies at different ends of a fiber. Red indicates the binding of anti-rabbit (Texas red labeled); green indicates binding of anti-mouse (FITC labeled). (b) The GFP antigen is observed to bind to the anti-GFP presenting fiber on the right while little GFP binding is observed for the control fiber at the left. The anti-GFP presenting fibers were prepared by sequentially incubating the chitosan fibers in solutions containing: tyrosinase plus the HG3T protein; the anti-GFP antibody, and the GFP antigen. Control fibers were prepared by deleting tyrosinase from the HG3T-assembly step. (c) Antigen binding as a function of fiber length (R^2=0.993) suggests antigen-antibody binding is not confined to the external fiber surface (see text). Antigen (i.e., GFP) binding was analyzed after dissolving the fiber in mild acid. (d) Simultaneous capture of two antigens by meshes woven from anti-GFP presenting fibers (vertical) and anti-BSA presenting fibers (horizontal). The mesh was immersed in a solution containing both the GFP and labeled-BSA antigens.

There may be applications that employ fibers for antigen capture (e.g., for environmental sampling), hence it would be desirable for the antibody assemblies to be stable in air for moderate amounts of time. To test for stability, we prepared chitosan fibers and sequentially assembled HG3T, anti-GFP antibody, and the GFP antigen. Resulting fibers were then rinsed and dried at room temperature. Fluorescence images of these air-dried fibers were obtained on the first and seventh days (Figure 2-7). Image analysis of the fiber's fluorescence intensity on the seventh day was estimated to be 95 % of that observed on the first day. Since GFP's fluorescence requires its native structure,

the above analysis suggests that this antibody-antigen assembly on the chitosan fiber is stable to room temperature storage in air.

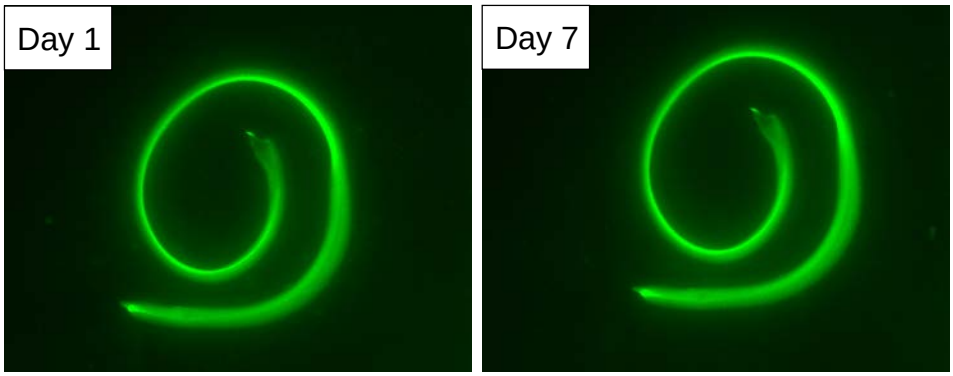

Figure 2-7 Stability of antigen-antibody assembly on chitosan fibers. Fluorescence images of these air-dried fibers were obtained on the first and seventh days. Image analysis of the fiber fluorescence intensity on the seventh day was estimated to be 95 % of that observed on the first day.

2.4. Conclusion

These studies demonstrate the use of three biologically-based fabrication methods for the hierarchical assembly of antibodies and antigens into macroscopic systems. We created tryosine tagged protein G that offers a biologically-activatable interface between the antibodies and the pH-responsive chitosan that, in turn, can be cast, electrodeposited, and spun into various geometries. Importantly, these biofabrication methods are simple and selective. The results also suggest potential applications. The chip studies show electrical signals can be enlisted to direct assembly, and suggest the potential for assembling antibodies at electrode addresses embedded within fully packaged microfluidic devices [116]. The fiber studies demonstrate high levels of antigen-antibody binding, and suggest the potential for antigen capture by smart fabrics. Potentially, biologically-based fabrication methods will provide a broader range of options for the hierarchical assembly of nanoscale components into novel materials.

Chapter 3. Autonomous bacterial dirigibles – new synthetic biology platforms for "smart" sensor-actuator devices

3.1. Introduction

The emerging practice of using bacteria as disease therapy vectors is gaining attention [28-30], even to the extent of a hypothesized alternative to anti-cancer agents such as standard chemo- and radiation- therapies [35-40]. To date, many genera of bacteria, including *Salmonella*, *Escherichia*, *Clostridium*, and *Bifidobacterium* have exhibited potential as cancer treating agents [32-34]. Indeed, Forbes (2010) [41] recently suggested characteristics of the ideal bacteria agent but did not describe innovative approaches that use the bacteria to make decisions that would enable autonomous delivery of disease-arresting therapeutics only to cancerous cells and not others.

Bacteria naturally move and make decisions; programming these functions using synthetic switches has only recently appeared. Cheng *et al*. [29] demonstrated the *in vitro* use of engineered strain of *E. coli* bacteria to kill pathogenic *P. aeruginosa* by producing pyocin S5, a protein antibiotic in response to the presence of signaling molecules generated from *P. aeruginosa*. The resulting pyocin S5 lead to the eradication of both *P. aeruginosa and* engineered *E. coli*. March *et al*. [28] showed the potential of using an engineered bacterial that produces cholera signaling molecule autoinducer 1(CAI-1) as a live vaccine. They prevented *Vibrio cholerae* virulence in an infant mouse model. These reports creatively exploit the natural signaling processes among bacteria and also reprogram their genetic circuits to generate user-specified positive outcomes. What is

missing thus far are innovative measures to use high level functions of the bacterial cells that might enable them to accomplish even more.

In this research, we demonstrate an innovative approach employing “smart” bacteria for the potential use in treatments of cancer and other diseases [41]. We generate a motile bacteria can provide both the means to find tumors, dock on associated receptors (“features”), integrate feature density, and then *decide* whether or not to take an action.

This novel “smart” bacteria reinforces the notion of an expanding “Synthetic Biology” umbrella. The general concept of synthetic biology encompasses the rewiring of a cell’s genetic circuitry for the synthesis of novel products using heterologous processes. In this approach, typically all cells carry out the same function. A less commonly examined but equally innovative strategy uses the reprogrammed cell as the product. This report falls under the latter category. Here we describe the synthesis and characterization of a modified *E. coli K-12* whose behavior is governed by a synthetic genetic circuit which endows tunable targeting, sensing and switching capabilities. The resultant cell is a bacterial “dirigible” – a cell that autonomously navigates and carries or deploys important “cargo”. Using biomarkers, receptors, or other mammalian cell surface features, these dirigibles can target specific locales. Sufficient accumulation at the target surface triggers an “on” switch in response to the biomarker density. This serves as a phenotype “focusing” system and maintains the switch in an “off” state until the desired threshold is reached (Figure 3-1).

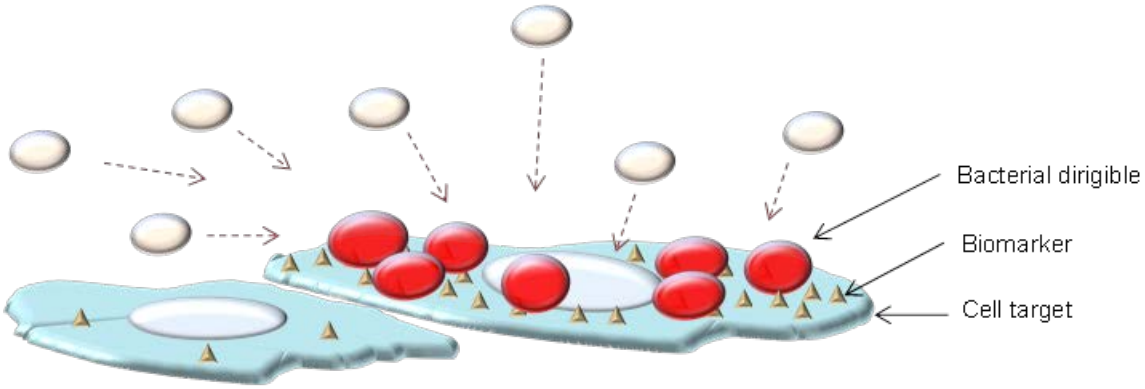

Figure 3-1 Schematic plot of the bacteria "dirigible" model. Bacteria targeting and switching are based on "feature" receptor densities of mammalian cells. Bacteria cells will potentially dock onto mammalian cells with high feature density and subsequently turn on the switch if the feature density reaches the threshold.

The dirigible's switching capability relies upon bacterial quorum sensing (QS), a density-dependent cell-cell communication process among bacteria that is mediated by the transmission and propagation of chemical signals known as "autoinducers" [117, 118]. Autoinducers are synthesized within the cell cytoplasm, secreted to the outside and accumulate in the cells' immediate surroundings [119]. At a point associated with a "quorum" of cells, where the cell density and hence the concentration of the exported autoinducer reaches a threshold, the signaling molecules are transported back into the cells or are bound to cognate cell surface receptors, where they initiate coordinated changes in gene expression [50]. Several classes of signaling molecules and QS mechanisms have been identified [118, 120]. This work leverages the transduction of autoinducer-2 (AI-2) signaling which is the dominant form of bacterial cell-cell communication in *Esherichia coli* and *Salmonella typhimirium*, among other bacteria.

Specifically, we genetically rewired the *E .coli* W3110 QS circuitry by knocking out *lsrF* and *LsrG* (AI-2 degradation genes), and co-transformed QS responsive plasmids [54] for enhancing AI-2 sensing and actuating capabilities (Fig 3-2a) as compared to wild type. In addition, we also utilized biological nanofactories (NF) (enzyme-based AI-2 synthesis device comprised His tag, protein G, LuxS, Pfs, and Tyr tag) facilitate AI-2 production [121]. Furthermore we integrated our modified bacterial "switch" with localization capabilities through two distinct, but complementary mechanisms. First, we engineered bacteria to contain a generic scaffold for antibodies which provides specificity in binding to surfaces of interest (chips/mammalian cells). Subsequent to dirigible targeting with antibody-nanofactory complexes, gene expression is turned on through a QS switch mechanism when sufficient AI-2 has been synthesized. The second approach utilizes nanofactory AI-2 synthesis to drive chemotaxis which guides bacterial homing and also eventually turns on gene expression. We demonstrate the feasibility and functionality of both switches using an *in vitro* cancer model as a target and discusses potential applications for cancer or other disease treatments.

3.2. Materials and Methods

Cell strains and plasmid construction

E. coli K-12 W3110 (*lsrFG*$^-$, *luxS*$^-$), generated using a one-step inactivation method [122], was the strain used throughout unless otherwise specified. This strain responds to a significantly lower AI-2 concentration than wild type W3110 (Figure 3-2a). Squamous cell cancers of the head and neck, PCI-15B (provided by Dr. Jennifer Grandis, Univ. of Pittsburgh) that expresses EGFR at high levels, was chosen for the bacterial targeting; HEK293 (human embryonic kidney cell, ATCC number: CRL-1573) was used as the corresponding control for its low expression of EGFR. Both PCI-15B and HEK293 cells were cultivated in Dulbecco's Modified Eagle's Media (DMEM) containing glucose (4.5 g/L), GlutMAX™ I (3.97 mM), and 10% fetal bovine serum (FBS, Sigma) at a 37^{o}C incubator supplied with 5% CO_2.

To construct plasmid pET-DsRed_tac-ompAG1, which encodes DsRed and surface displayed protein G, we performed PCR to amplify the surface display fragment including outer membrane protein A and signal-peptide (lpp-ompA) using the template vector pTX101 (provided by Dr. George Georgiou, Univ of Texas, Austin) [123] and protein G fragment using the pET32-G3T vector[47]. Subsequently, a fusion of lpp-ompA and a protein G gene fragment containing a Hind III site was generated again by PCR and then inserted into pET-DsRed with Hind III (NEB) ligation. The resulting plasmid product was then co-transformed along with pCT6 [54] vector into W3110 (*lsrFG*$^-$, *luxS*$^-$) (Figure 3-2b).

Bacteria response to in vitro AI-2 production

For creating differential antigen surface densities, various concentrations of avidin (Rockland immunochemicals) were added to pre-treated biotin coated plates (Pierce). Anti-avidin (FITC) conjugated nanofactories with 1:2 weight ratio (1/200X dilution) were applied to guide the NF targeting toward the avidin surface.

Bacteria, as descripted above, were resuspended in Dulbecco's Phosphate Buffer (DPBS) (Sigma) containing 1mM S-adenosylhomocysteine (SAH; Sigma) and then incubated in the NF-treated plates. Bacterial response to AI-2 production was monitored via their fluorescence response using a plate reader (SpectraMax M2; Molecular Devices). *In-vitro* AI-2 concentration was measured via a stoichiometric proxy, homocysteine with the Ellman's assay.

Controllable protein G expression on bacteria surface

E. coli carrying plasmid pET-DsRed_tac-ompAG1 were induced with varied concentrations of IPTG (Sigma) and incubated at 37^{o}C shaking at 250 rpm for 1.5 to2 hours. Cells were harvested and incubated with anti-mouse DL488 (Jackson immunoresearch). Unbound antibodies were rinsed off and fluorescent images of bacteria taken to determine antibody conjugation efficiency or degree of protein G expression.

In vitro bacteria targeting and switching/actuating

E. coli cells were induced with 0.5 mM IPTG for 2 hours to express protein G followed by AF488 labeled mouse anti-EGFR (Santa Cruz Biotechnology) coupling.

Bacterial cells were then applied to a 96-well plate (Greiner Bio-One) cultivated with PCI-15B and HEK293 cells for EGFR targeting. The wells were washed with DPBS to rinse off unbound bacteria and then treated with goat anti-mouse coupled nanofactories. After washing with DPBS, an S-adenosyl-homocysteine (SAH) solution was added to the wells and bacterial fluorescence response was assessed over 12 hours.

Chemotaxis of in vitro synthesized AI-2

In vitro AI-2, SAH, and homocysteine (Sigma), were diluted into equivalent concentrations (40uM) with DPBS and then added into the top compartment of transwells (3um porosity; BD Biosciences) in 6-well plates (Corning). *E coli* cells resuspended in DPBS (OD_{600} ~0.15 to 0.2) were then applied gently into the bottom compartment surrounding and below the top compartment of the transwells. The plates were then incubated at 30^{o}C for 2 hours; bacterial cell density in the top compartment was assessed as a marker of cell motility.

Chemotaxis and actuation of bacteria in response to in situ AI-2 produced by locally targeted nanofactories

15B and HEK cells were seeded onto 1% gelatin treated glass slide (25mm round; Fisher Scientific) one day prior to experiments. NF and anti-EGFR were co-incubated for 30 mins (2:1 molar ratio) and then diluted into 1% BSA-DPBS (1ug/100ul). Afterward, the cells were treated with anti-EGFR-NFs for one hour followed by rinsing with DPBS 3X and placed into 1mM SAH (DPBS) containing transwells (3um porosity; 6 well plate formats). The glasses slides were incubated at 37^{o}C (in 5% CO_2) for three

hours followed by the addition of bacteria (OD_{600} 0.15-0.2 in DPBS) into the bottom compartment for extra 6-hour incubation. AI-2 production, bacterial migration, and actuation/response were examined by Ellman's assay, OD_{600}, and fluorescence microscopy respectively.

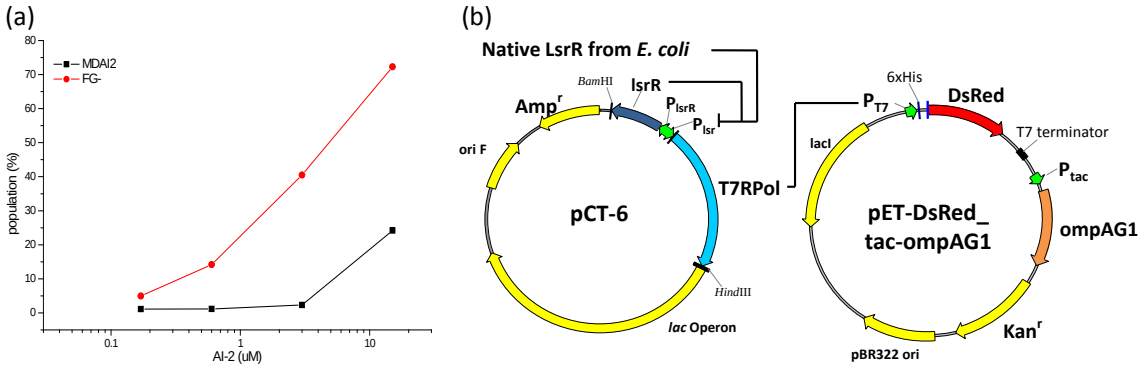

Figure 3-2 Characterization of W3110 (*lsrFG*$^-$, *luxS*$^-$) and construction of pET-DsRed_tac-ompAG1 vector. (a) AI-2 sensitivity of W3110 (*lsrFG*$^-$, *luxS*$^-$) vs. MDAI2 (W3110 (*luxS*$^-$)). Both bacteria cells carrying pCT-6 + pET-DsRed_tac-ompAG1 induced with various amounts of *in vitro* AI-2 concentrations for 8 hr. Subsequently cells were harvested and the positive DsRed population of bacteria in respond to AI-2 was measured by flow cytometry. The results suggest W3110 (*lsrFG*$^-$, *luxS*$^-$) is more responsive than MDAI2 (W3110 (*luxS*$^-$)). (b) Incorporation of QS vector PCT-6 with pET-DsRed_tac-ompAG1 to express DsRed and protein G in response to AI-2 and IPTG respectively.

3.3. Results and discussions

In order to create a "feature" surface for building the gradient of signaling molecules, two assembly strategies (synthetic and natural) are exploited for the assembly of gradient in binding molecules and cells. In a synthetic system, various densities of binding molecules are generated through protein biofabrication. In a natural system, different amounts of mammalian cells are seeded to form a gradient of surface bound receptors. Both naturally and synthetically created surfaces are investigated subsequently for the bacteria switch.

Antibody facilitated bacteria targeting and AI-2 generation

We created a gradient of avidin densities on a series of chips/wells to biotin-coated ELISA wells, depositing the target for FITC labeled rabbit anti-avidin conjugated HGLPT nanofactories (NF). As depicted in Figure 3-3a, the NF has the capability to convert SAH into AI-2 through the Pfs and LuxS enzymes. They also target antigens through protein G (IgG-binding motif, for antibody conjugation). A gradient of avidin was created in multiwell plates resulting in different levels of NF binding. This can be seen in Figure 3-2b where we both measured the level of NF binding and its corresponding AI-2 production as a function of avidin coated onto surfaces. A strong positive correlation between both curves was observed. That is, both curves were similar. Also, both curves achieved saturating signals at avidin levels above 50 ng. We inoculated these surfaces with SAH and bacteria W3110 (*lsrFG*$^{-}$, *luxS*$^{-}$) which carries vectors pCT6 + pET-DsRed_tac-ompA-proteinG in a 37^{o}C incubator. DsRed responses of bacteria samples were characterized by measuring the DsRed fluorescence with a plate

reader over time. As indicated in Figure 3-3c, the trends of all curves correlate to the NF binding (Figure 3-3b), that is, increased fluorescence with avidin. Time course curves indicate the overall DsRed intensities increased over time (8, 16, 19, and 26 hr), suggesting AI-2 concentration increased along the time frame in the experiment. While low DsRed was observed for the control sample without SAH at 26hr, suggesting no AI-2 was produced. The results depicted in Figure 3-2b and 3-3c, we demonstrated the ability to control the binding of NF to a specific surface through antigen-antibody interaction and calibrate subsequent AI-2 productivity. We also demonstrated the bacteria we engineered were capable of actuating DsRed gene expression in response to various concentrations of AI-2.

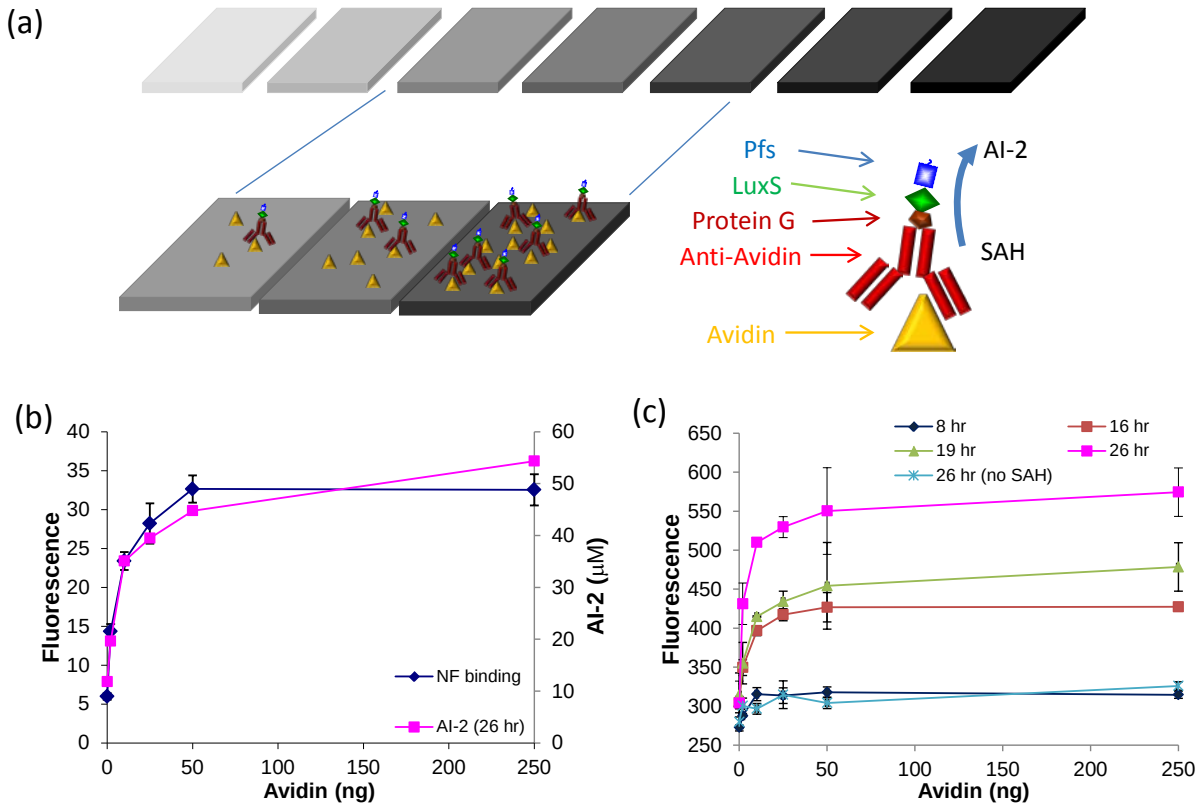

Figure 3-3 NF targeting and bacteria response on varied densities of avidin coated chips/wells. (a) Conceptual plot for NF targeting on various densities of avidin chips. NFs are fusion proteins comprised of Pfs, LuxS (for *In vitro* AI-2 synthesis) and protein G (IgG-binding motif, for antibody conjugation). Anti-avidin (FITC) coupled NFs target to avidin chips and catalyze SAH to AI-2. Note the chips here represent the biotin-avidin treated plate wells. (b) NF targeting and subsequent *in vitro* AI-2 syntheses on avidin plate wells. NF targeting was determined by a fluorescence plate reader (FITC) and AI-2 concentrations were measured by Ellman's assay. (c) W3110 (*lsrFG*$^{-}$, *luxS*$^{-}$) response to *in vitro* AI-2 synthesized by NF targeting on avidin plate wells. Suspension of bacteria was added directly to the wells and DsRed intensities were measured by the fluorescence plate reader.

Next, we developed a strategy to elucidate spatially-resolved "docking" of bacteria. We utilized the bacteria outer membrane protein A (ompA) as a transmembrane domain to display *Streptococcal* protein G on the outer cell surface. This allows ex vivo

assembly of potentially any antibody for targeting and "docking" bacteria to any specified surface. An ompA and protein G DNA fusion was PCR-amplified and ligated into pET-DsRed vector under the control of a *tac* promoter. In parallel, we created an AI-2 based expression control "cassette" and inserted DsRed as a marker. The resultant pET-DsRed_tac-ompAG1 vector (Figure 3-2b) was transformed into *E. coli* W3110 (*lsrFG*$^-$, *luxS*$^-$). The subsequent strain was capable of expressing protein G in response to IPTG and DsRed in the presence of AI-2. Figure 3-4 depicts the expression profile induced by varied concentrations of IPTG. Bacteria W3110 (*lsrFG*$^-$, *luxS*$^-$) which carries vectors pCT6 + pET-DsRed_tac-ompA-proteinG was induced by varied concentrations of IPTG (0, 0.05, 0.1, and 0.5mM). After 1.5~2hr induction at 37^{o}C 250 rpm shaking, the relative expression levels of protein G of bacteria were quantified. Through visualization afforded by DL488 labeled anti-mouse IgG staining, protein G expression level was titrated through both fluorescence images and flow cytometry (Figure 3-4a and 3-4b respectively). The DL488 fluorescence intensities increased with IPTG suggests the increase of protein G expression level in both Figure 3-4a and 3-4b, while minimized DsRed were observed in Figure 3-4a. This tunable expression of surface displayed protein G enables titration of avidity to targets of interest.

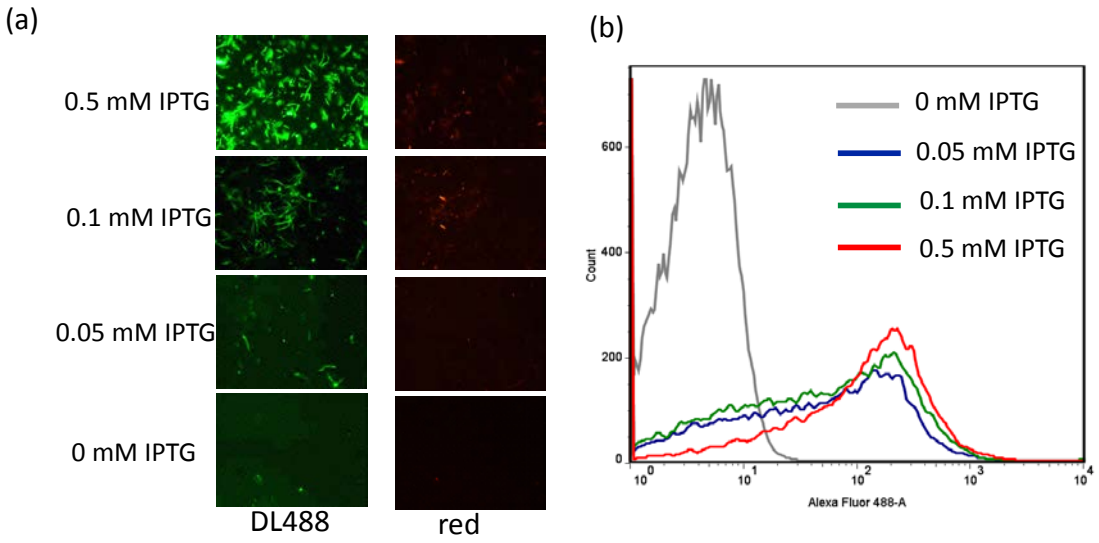

Figure 3-4 Tunable protein G expression from W3110 (*lsrFG*$^-$, *luxS*$^-$) carrying vectors pCT6 + pET-DsRed_tac-ompAG1. Protein G expression profile was determined by inducing with varied concentrations of IPTG. After 1.5~2hr induction, the relative expression levels of protein G of bacteria were quantified. Through visualization afforded by DL488 labeled anti-mouse IgG staining, protein G expression level was titrated through both fluorescence images (a) and flow cytometry (b).

We hypothesized that the engineered bacteria could both target and actuate by using a "smart" switching functionality. The cells were equipped with FITC labeled anti-avidin by protein G conjugation. These complexes were then applied to the avidin pre-treated biotin plate (same avidin setup as Fig 3-3a). Next, 40uM *in vitro* AI-2 was added to the targeted cells and DsRed responses were measured after 12 hours. In Figure 3-5a the assembled cell number (indicated by green fluorescence) increased with avidin. As depicted here, images from the 0 hour time point suggest the amount of *E. coli* targeting is positively proportional to avidin density on the plate (FITC channel) except the 250ng well, where binding may have already plateaued. Moreover, the cells only expressed low background level of DsRed initially. After 12 hours, however, cells incubated with AI-2

were significantly more fluorescent compared to those without AI-2. In addition to the qualitatively observation, we further performed the particle analysis using ImageJ software for further quantitation. As indicated in Fig 3-5b again, a linear relationship between bacteria docking and avidin density were observed for all curves, FITC (0hr), DsRed (0hr), and DsRed (12hr; with AI-2 addition) at avidin density less than 50ng. The FITC (0hr) curve matched comparably to the DsRed (+AI-2; 12 hr) which suggests most of the docked bacteria basically were switched on after AI-2 addition. Almost no DsRed cells were observed in the treatment without AI-2 after 12 hr. And interestingly, the number of DsRed positive cells at 0 hr time point was slightly higher than cells that without AI-2 addition at 12 hr (39 vs 6) and the reason is not known. However, we speculated that DsRed was metabolized or degraded after 12 hr without any new DsRed synthesized. Overall, we demonstrate the cells can target and then subsequently actuate in the presence of AI-2.

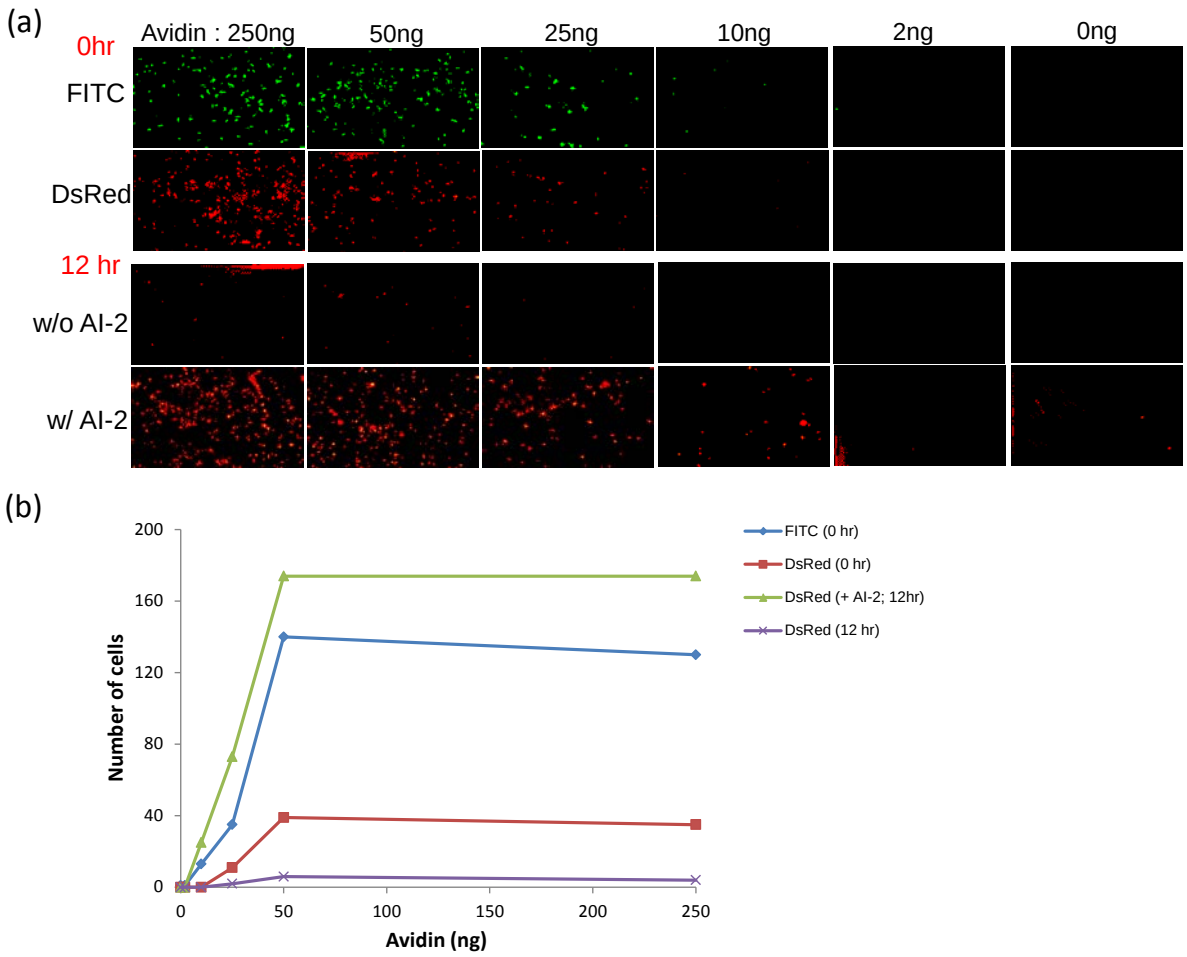

Figure 3-5 AI-2 response of docked W3110 (*lsrFG*$^{-}$, *luxS*$^{-}$) (pCT6 + pET-DsRed_tac-ompAG1) on avidin coated wells. (a) W3110 cells with surface displayed protein G were treated with FITC labeled anti-avidin and then applied to various densities of avidin wells. Unbond bacteria were washed followed by 40uM AI-2 addition. Fluorescence images at 0 and 12 hours were taken by fluorescence microscopy. (b) Image analysis of Figure 3-5a using ImageJ to determine the bacteria number targeted on the avidin surfaces. The relationship between cell number and avidin density was plot.

To test the integration of all these elements, we selected two mammalian cell lines, PCI-15B and HEK293, as our surfaces of interests for their contrasting high and low expression of EGFR, respectively. As indicated in Figure 3-6a, we first seeded both PCI-15B and HEK293 in 96-well plates at varied density. Next, we prepared W3110 cells with mouse anti-EGFR coupled to their surfaces followed by applying the bacteria cells

to the PCI-15B and HEK293 cells cultivated in 96-well plates for targeting. Subsequently, goat anti-mouse conjugated nanofactory complexes were directly bound to bacteria cell surfaces to assist in tuning the switch. Finally, we added SAH into the wells and incubated at 37^{o}C in 5% CO_2 for 12 hours to test whether the bacteria docked onto eukaryotic cells could respond to AI-2. As shown in Figure 3-6b, the fluorescent and bright field images indicate that the anti-EGFR-bacteria bind specifically to the cell surfaces of interest. The staining on the HEK293 monolayer is significantly less than that on the PCI-15B monolayer. After a 12-hour incubation with SAH (Figure 3-6c), the bacterial cells turn on DsRed expression on PCI-15B only at the two highest mammalian seeding densities (20,000 and 10,000 cells/well). DsRed expression indicates the QS switch was "on". Wells with low PCI-15B densities or without NF treatment had minimal DsRed expression, similar to the HEK293 control cell surface. We further processed the image data from anti-EGFR-bacteria binding (Figure 3-6b) and DsRed response (Figure 3-6c) experiments using ImageJ and resulted in Figure 3-6d and Figure 3-6e respectively. As the NF complexes were applied in excess for these experiments, the amount of NF attached to the mammalian target surface was assumed to be directly proportional to the bound bacteria population. As seen in Figure 3-6d, a linear relationship between fluorescence of AF488-anti-EGFR (bacteria number) and mammalian cell density was observed for cell seeding densities below 10,000 after which point the signal saturates. This bacteria number- to-mammalian density linear relationship was not, however, reflected in the switching response, which as shown in Figure 3-6e, was kept tightly off until the cell seeding density reached 10,000, at which point DsRed expression was turned on. This indicates the QS switching here has a

threshold limit for actuation directly related to EGFR “feature” densities. We envision this engineered *E. coli* could potentially be used in conjugation with NF as a relatively safe switch with a relatively high threshold and low background *in vitro* or *in vivo*.

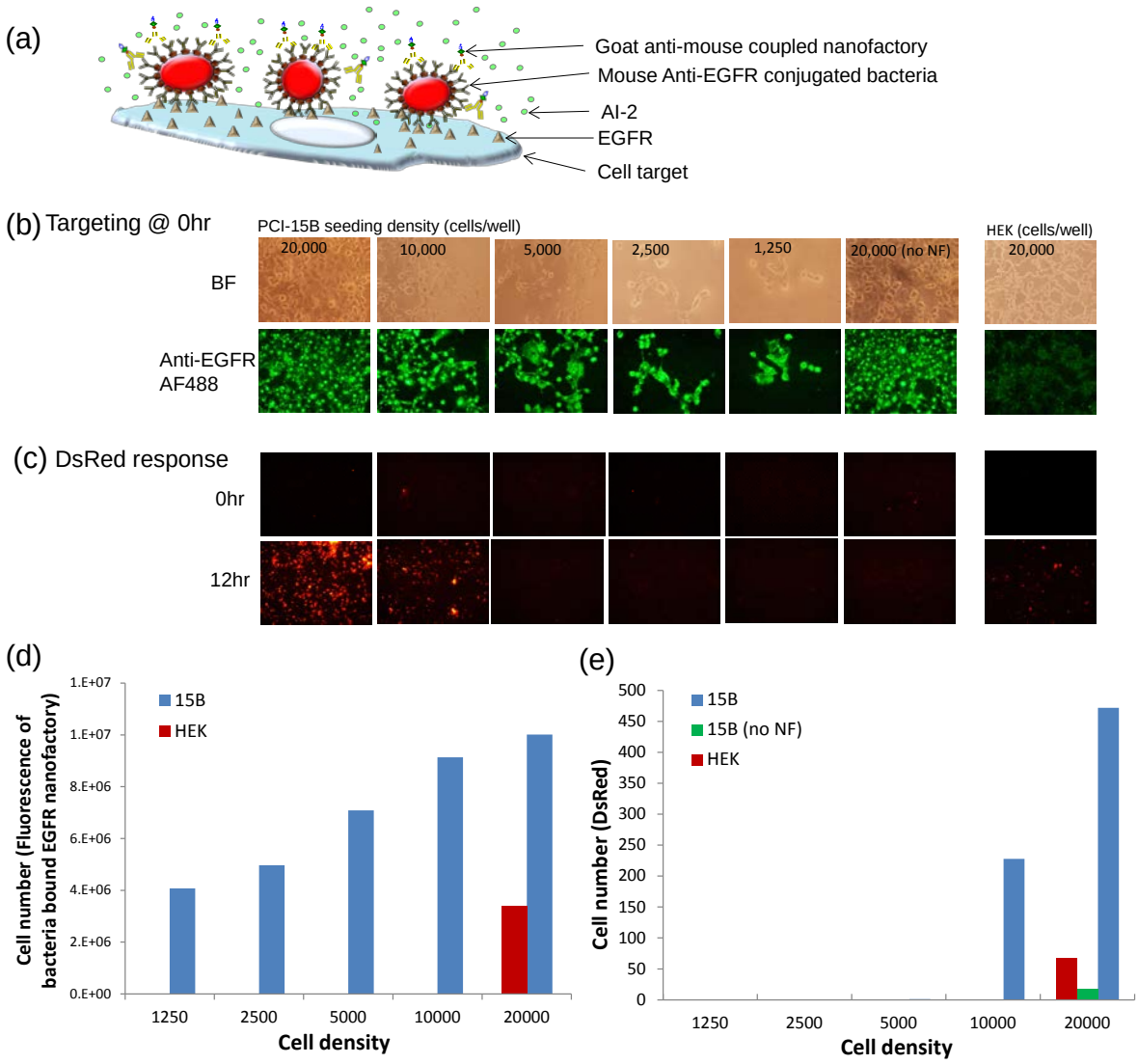

Figure 3-6 W3110 (*lsrFG*$^{-}$, *luxS*$^{-}$) (pCT6 + pET-DsRed_tac-ompAG1) targeting and actuating on mammalian cell surface. (a) Scheme of bacteria targeting to receptors of mammalian surface and subsequent NF conjugation to targeted bacteria for locally AI-2 synthesis and delivery to trigger bacteria switches. The procedures are as follow: anti-receptor Ab coupled bacteria (through prtein G) target to EGFR on cell surfaces, secondary Ab-NFs target to bound bacteria, and NFs convert SAH into AI-2 for bacteria actuation. (b)As indicated in (a) various densities of PCI-15B or HEK cells were seeded to wells followed by mouse anti-EGFR (AF 488 Labeled) bacteria, anti-mouse-NF targeting and subsequent SAH addition. (c) Bacteria responses/ DsRed expression were measured after 12 hour incubation. (d) Further analyses of images from (b) to obtain the correlation curve between mammalian cell seeding densities and amount of bacteria/NF binding. ImageJ was utilized to determine the AF488 fluorescent intensities. (e) Relationship between bacteria responses and cell densities were investigated to determine the threshold of the switch.

AI-2 guided bacteria homing and actuation

A second strategy to assess bacteria localization is to decorate the target feature itself with NF, and synthesize AI-2 directly at the target to attract bacteria by exploiting native bacteria AI-2 chemotaxis. First, to test whether AI-2 is a chemoattractant for *E. coli* K-12 W3110, experiments were conducted with a transwell setup to allow AI-2 diffusion across the membrane generating a concentration gradient. 40uM *in vitro* AI-2 was added to the top, luminal transwell compartment and W3110 to the bottom, basolateral compartments in 6-well plates. The transwell containing plates were incubated for 2 hours at 37^{o}C with no shaking. AI-2 diffusion was simulated using a finite element modeling method with a diffusion coefficient of $3x10^{-8}$ to confirm gradient formation. Simulation results from Figure 3-7a showed the pattern of gradient formation was similar between the duration of 1hr and 2hr time point, suggesting that the limiting dimensions between transwell compartments prevent gradient dissipation during the relevant experimental time frame. After 2 hr incubation, optical densities (OD_{600}) of both top and bottom compartments were measured to determine the number of migrated bacteria. Cell counting was performed by taking bright field images of the top compartment samples. As shown in Figure 3-7b, the cell density in AI-2 sample was significantly higher than SAH sample, indicating AI-2 was effectively attracting more bacteria. Similar results (Figure 3-7c) were seen for OD_{600} measurements, in which the *in vitro* AI-2 induced chemotaxis. The OD in top AI-2 well was initially 2.8-fold of SAH and significantly increased to 34-fold after 2 hr incubation. The OD of bottom SAH well did not change after a 2-hour incubation, while the AI-2 bottom well dropped significantly by 30%. In another experiment (Figure 3-8), we tested several other buffers,

including homocysteine (a by-product of AI-2 synthesis), Tris-HCl, and DPBS and reconfirmed that AI-2 was the only chemoattractant in our design experiments.

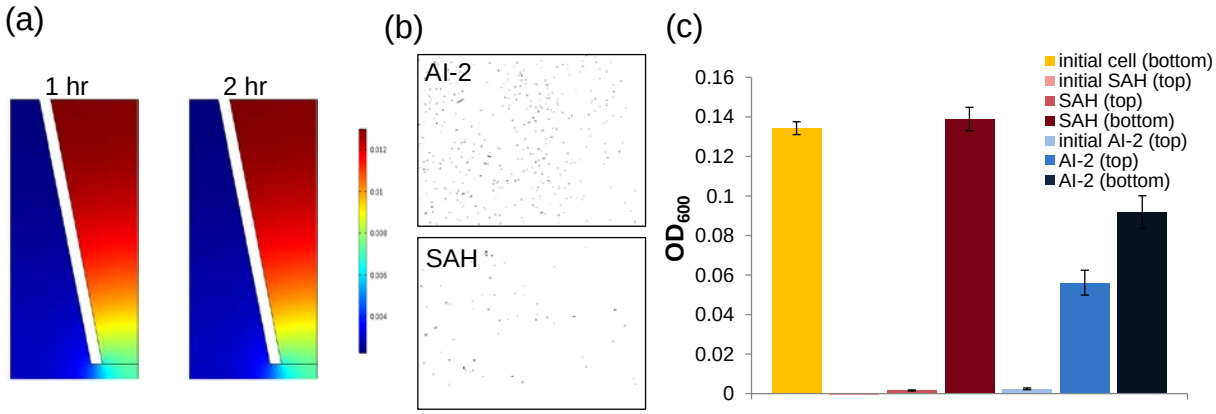

Figure 3-7 AI-2 chemotaxis on *E. coli* W3110 (*lsrFG*$^-$, *luxS*$^-$) (pCT6 + pET-DsRed_tac-ompAG1). (a) Simulation of i*n vitro* AI-2 diffusion profile across the transwell membrane (from top to bottom) using COMSOL software. Chemotaxis experiment was performed as followed. 1.5ml of *in vitro* AI-2 and SAH (40uM) was added into top parts of the 3um -6 well inserts. Bacteria cells (OD~ 1-1.5) rinsed with DPBS three times were then resuspended into DPBS (OD ~0.2-0.3) and applied into bottom wells. The inserts were incubated static at 37^{o}C for 2 hours. Bright filed images of cell migrated to top well were taken (b). And a systematic OD characterization was conducted for the bacteria migration from bacteria source (bottom) toward chemoattractant (top).

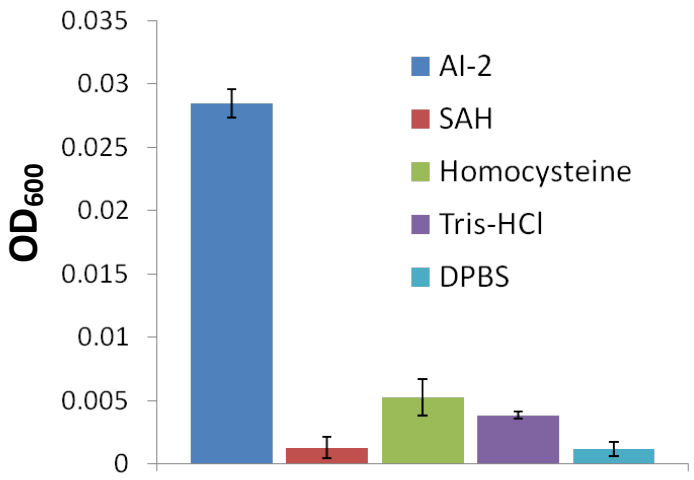

Figure 3-8 Effect of AI-2 and relevant chemicals on W3110 (*lsrFG*$^{-}$, *luxS*$^{-}$) (pCT6 + pET-DsRed_tac-ompAG1) chemotaxis. Equivalent molar concentration (40uM) of AI-2, SAH (precursor of AI-2), Homocysteine (side product of in vitro AI-2 synthesis), and buffer (DPBS, Tris-HCl) were tested for chemoattactants. 1.5ml of Samples was added into top parts of the 3um -6 well inserts. Bacteria cells (OD~ 1-1.5) rinsed with DPBS three times were then resuspended into DPBS (OD ~0.2-0.3) and applied into bottom wells. The plates were incubated static at 37^{o}C for 1.5 hours. OD of the bacteria inside the insert was measured afterward.

We demonstrated that NF production of AI-2 at the mammalian cell surface is capable of attracting bacterial cells in response to the AI-2 gradient and subsequently triggering “dirigible” switching behavior. A schematic of this experimental setup is depicted in Figure 3-9a.We first seeded the mammalian cells (15B and HEK) on gelatin coated glass coverslips, introduced anti-EGFR- NF complexes and applied SAH into the top transwell compartment. We placed the gelatin coverslip upside-down to face mammalian cells toward bacteria. The W3110 cells were added into the lower wells afterward. After 9-hr incubation of the transwell setup, we checked whether the bacteria will be able to migrate toward up and then target to mammalian surfaces by measuring OD, *in vitro* AI-2 concentration , as well as taking fluorescence images. After selectively

targeting NF to the surface of interest (green images of Figure 3-9b), AI-2 was locally synthesized adjacent to the mammalian cell surface (15B and HEK) creating a concentration gradient, which attracted bacteria chemotactically as an analogous "homing" signal. Compared to 15B cells, HEK cells showed less green EGFR binding (similar to Fig 3-6b). The resulting differential DsRed bacteria observed on the red channel images suggest different amounts of bacteria migrated up and across the transwell barriers (Figure 3-9b). For 15B+SAH well, high density of DsRed bacteria was observed as compared to 15B+PBS, almost no DsRed bacteria. Also, few DsRed-expressing bacteria were seen on HEK+SAH. The results correspond to the AI-2 concentration profile (Figure 3-9c) and OD measurement of the bacteria cell density in top well (Figure 3-9d). As Indicated, the highest bacteria density was observed in the wells treated with 15B+SAH and lowest in 15B+PBS treated wells. Importantly, a significantly higher density of dirigibles also displayed switch responses in the 15B+SAH wells compared to the HEK+SAH wells, while a minimal switching density was observed in 15B+PBS control wells. Interestingly, the *in-vitro* AI-2 quantified in 15B+SAH sample was 5uM which corresponded to the previously determined threshold for QS switch [121]. Note here that AI-2 played a dual role both guiding bacteria chemotaxis and also triggering the switching response (DsRed reporter expression, Figure 3-9b). In summary, the docking of anti-EGFR-NF onto mammalian cell surfaces was specifically controlled by EGFR surface density which strongly correlated to subsequent AI-2 synthesis, bacteria migration, and switching response phenotypes.

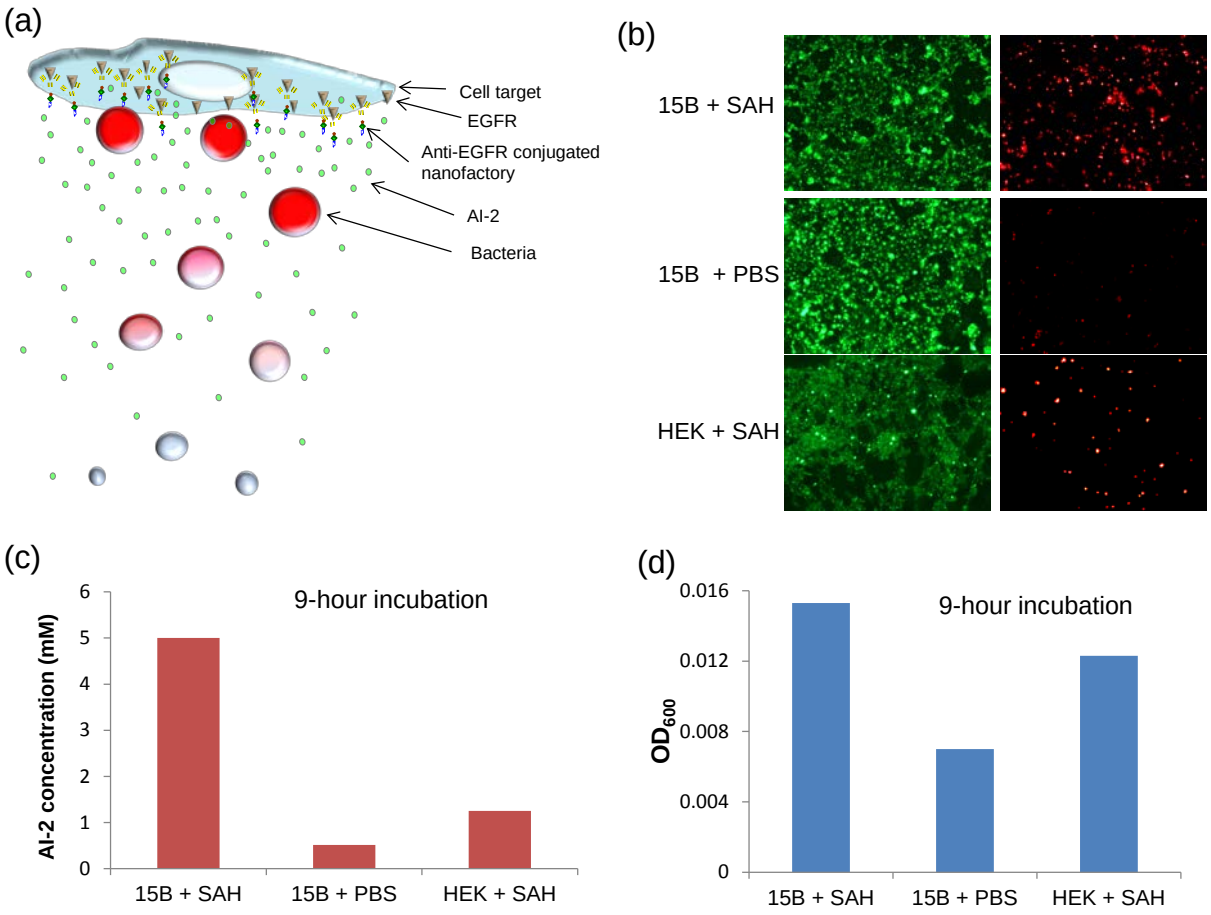

Figure 3-9 Bacteria chemoattraction and actuation through AI-2 synthesis of NF. (a) Bacteria switch: schematic represents the targeting of NF to surface of interests, e.g. cancer cell surfaces, AI-2 production locally on the surfaces, AI-2 gradient through random diffusion, and then subsequent bacteria attracting and actuating. Mammalian cell surface is facing upside down in order for bacteria migrating toward them in the transwell configuration. (b) Results of the bacteria switch: anti-EGFR-NFs binding to EGFR on both 15B and HEK cells were shown on the AF488 (green fluorescence) images and bacteria attracting, docking, and DsRed expression were presented on the red fluorescence images. Corresponding AI-2 production was determined by Ellman's assay (c). Amount of attracted bacteria were measured as the OD inside the insert (d).

3.4. Conclusion

We demonstrated the use of engineered bacteria with a rewired quorum sensing circuit as a potential dirigible switch, the features of which comprise targeting, sensing, and actuating capabilities. We have created and tested two complementary targeting or localization schemes to demonstrate dirigible switching on mammalian cell targets in an in vitro cancer model. First, dirigibles and nanofactories were independently and specifically bind to the mammalian cell surface. Bound bacteria could sense and respond to locally synthesized AI-2 by the nanofactories. Additionally, we also carried out a second dirigible strategy leveraging the AI-2 produced by the docked nanofactories as a homing signal for attracting dirigibles (chemotaxis) and actuating the dirigible phenotype switch. For both targeting and localization schemes, the dirigible response was controlled by AI-2 concentration, which primarily depended on the cell receptor, or "feature" density. The higher feature densities on 15B cells allowed more nanofactories to dock, thereby increasing the effective local AI-2 concentration. Correspondingly, the overall densities of triggered bacteria were significantly more on 15B surfaces than comparative HEK293. The mechanism provides a reasonable and discernible means to ensure site specific actuation, providing a more focused and effective phenotype. We envision this novel bacterial dirigible scheme, that integrates both targeting and switching, could potentially provide a relatively safe means for cancer or disease treatment.

Chapter 4. Tuning cell cycle of insect cells for enhanced protein production

4.1. Introduction

There exists great promise for whole promise genome engineering for the production of both commodity products and high value therapeutics, that enable glycoprotein expression and purification from *E. coli*[124] , particularly when coupled with the considerable power of bacterial genome engineering [125], hold promise to transform the commercial protein synthesis landscape.

The integration of innovative molecular tools to metabolically engineer cells for expression of expression of recombinant proteins has and will continue to afford significant gains, particularly if both localized genetic circuits and global regulatory structures can serve to guide fluxes through specific bottlenecks in the context of a favorable landscape, respectively. Both synthetic and altered native controllers are developed to guide protein synthesis, many transcending the host cell system. In eukaryotic (mammalian, insect) cell systems, which provide superior glycosylation capabilities, interfering RNA (RNAi) is used to target local bottlenecks [75] as well as global processes [126].

Eukaryotic cell cultures remain the main sources for the production of pharmaceutical proteins despite their relatively low growth rate and protein yield as compared to prokaryotic expression systems [25-27]. This is mainly due to the enhanced quality of the product protein [47, 127]. Low mammalian cell growth rates and yields are due to a complicated network of regulatory mechanisms that monitor and check their internal physiological conditions, metabolic activities, as well as the absence of external

signals as a precondition to cell proliferation [128-130]. These cells progress through chromosome duplication and cell division in a process called the “cell cycle”. The cell cycle consists of many checkpoints during which certain conditions must be met before passing to the next stages. This strategy which ensures cell integrity and survivability can, however, sometimes compromise growth rate and protein synthesis. Since cell cycle and proliferation status are closely related to protein synthesis activity [63, 131-133] the cell cycle is a potential metabolic engineering target. Metabolic engineering approaches to arrest the cell cycle at specific states have been demonstrated as advantageous for recombinant protein production in eukaryotic cells [127, 134, 135].

The eukaryotic cell cycle can be divided into four distinct phases: gap-1(G1), DNA synthesis (S), gap-2 (G2), and mitosis (M) [127, 136]. Cells arrested at G1 (protein synthesis) phase have been shown to exhibit the highest ribosome biogenesis and protein translation activity of any cell cycle phase, resulting in higher recombinant protein yields [64, 137]. In G1 phase, cell resources are utilized more efficiently for synthesizing proteins of interests without diverting energy to produce cell components for proliferation [134, 135, 138]. For example, Bi et al. (2004) [139] showed that over-expression of the cyclin-dependent kinase inhibitor p21 causes G1-phase cell cycle arrest in Chinese hamster ovary (CHO) cells. These G1-arrested cells showed an increase of mitochondrial mass and activity as well as ribosomal protein S6 translation levels, culminating in a 4-fold increase of recombinant protein productivity. Although cell cycle control has been demonstrated in mammalian cell lines for recombinant protein production, few studies have examined the feasibility in insect cell expression system. March and Bentley (2007) [75] successfully arrested cells in G1 phase and increased the target GFP production by

4-fold in *Drosophila* S2 cell line using dsRNA technology (RNA interference) to knockdown the *cyclin E* (positive regulator for G1-to-S phase) expression. This study is, as far as the authors are aware, the only reported use of RNAi approaches to control the cell cycle and recombinant protein production in eukaryotic cells. We therefore found it worthy to pursue such an approach in a more industrially relevant insect cell line, such as the High Five cell line derived from the cabbage looper (*Trichoplusia ni*).

In this research, we use a dsRNA knock down strategy against *Trichoplusia ni* (*T. ni*) *cyclin E* (*CycE*) to manipulate the cell cycle of *T. ni* cell line. In normal cell proliferation, Cyclin E is regulated so that a natural increase and subsequent decrease guides the G1 to S transition [133]. Hence, our hypothesis is that altered CycE level can lead to alter cell cycle decision-making process and that lead to altered phenotype. Specifically the sustained up-regulating of CycE leads to over-proliferation. Also down-regulating of CycE would essentially stall the transition S phase from G1. Thus we investigate the effect of cell cycle regulation on both cell physiology and protein production in *T. ni* (High Five) cell cultures using the baculovirus expression system. Specifically, we identified the complete *T. ni* CycE genetic sequence, then up-regulated *CycE* expression by transfecting High Five cultures with an expression vector carrying *CycE*. Next, the *CycE* gene expression was down-regulated via dsRNA against *CycE*. For both experiments, *CycE* transcription level, cell growth, as well as cell cycle distribution were examined. Finally, the dosage-dependent effect of dsCycE on recombinant protein production using the baculovirus expression system was examined.

4.2. Materials and Methods

Cell culture

T. ni BTI-TN-5B1-4 (High Five™, Invitrogen) cells were cultivated in EX-CELL™-405 media (SAFC Biosciences) at 27 °C in T75 flasks (Corning) for adhesion culture. Cells were also adapted to suspension culture by cultivated in 125 ml shaker flasks (Corning) with ~120rpm at room temperature. Cell passage was conducted every two to three days, or whenever cell density reached confluency or (2.5~3 million cells/ml), and then split into 0.6 to 0.8 million cells/ml.

Baculovirus amplification and Infection

A recombinant *A. californica* multiple nucleopolyhedrovirus (AcMNPV) that expresses GFPuv under the control of the polyhedron promoter was created previously [140]. The baculovirus was amplified in *S. frugiperda* (Sf-9) cells (Invitrogen) according to the standard protocols with MOI (=0.1) and harvested the supernatant of cell media after centrifugation. Baculovirus titer was determined by the endpoint dilution with GFPuv fluorescence measurement using a fluorescence microscopy (BX60; Olympus), a plate reader (SpectraMax M2; Molecular Devices), or flow cytometry (FACSCanto II; BD Biosciences).

Identification of CycE sequence

In order to determine the initial putative primers sequences for RT-PCR, *CycE* sequences among inter-interphylum species were collected from NCBI Genbank and multiple sequences alignment was performed by Clustal X software (EBI) to obtain the

consensus regions and subsequently the degenerate primers for PCR were designed as 5'-GARGARATYTAYCCNCCHAAR-3' (R: A/G; Y: C/T; N: A/T/C/G; H: A/T/C). Next, RACE RT-PCR was performed with the degenerate primers. Briefly, total RNA of High Five cells was extracted using RNAquous (Ambion) followed by reverse-transcription via SMART-RACE cDNA amplification kit (Clontech). The resultant PCR products were ligated into TOPO TA vector (Invitrogen) and subsequent DNA sequencing was carried out by IBBR sequencing facility (DNA sequencer 3730; Applied Biosystems) to obtain the *T. ni CycE* cDNA sequence.

pIB-TnCycE vector construction

CycE gene was first PCR amplified using accuprime Hi Fi polymerase (Invitrogen) and TOPO-ligated into pIB/V5-His vector (Invitrogen) to generate pIB-TnCycE vector. The ligation products were transformed into *E. coli* TOP 10 competent cells (Invitrogen) and then plated to LB/agar (Fisher Scientific) with Kan 50 ug/ml at 37^{o}C for overnight growing. Single colony of cells was picked and inoculated into LB broth (Fisher Scientific) with Kan 50 ug/ml at 37^{o}C 250 rpm for overnight. Plasmids were purified with miniprep kit (Qiagen) and the concentrations were quantified by NanoDrop (Thermo Scientific). DNA sequencing of CycE insertion was carried out to confirm the success of the cloning works.

In vitro double stranded RNA (dsRNA) synthesis

In vitro dsCycE was synthesized using the Megascript Kit (Ambion). T7 promoter sequence was incorporated to both 3' and 5' end of partial *CycE* fragments by

PCR with primers which had extra T7 promoter overhang. *In vitro* transcription of dsCycE (800 bp) was then generated according to the manufacture instruction. Briefly, the single stranded CycE was synthesized and then extracted using phenol/chloroform (Sigma) followed by resuspending in nuclease free water. Subsequently, ssCycE was re-annealed into dsCycE by denaturing at 65^{o}C for 10 min and then slowly cooling to room temperature. Double stranded chloramphenicol acetyl transferase (dsCAT) was generated the same procedures and served as nonspecific dsRNA for control dsRNA treatment.

Transfection

RNAi or plasmid vector delivery was carried out by utilizing a transfection reagent Fugene HD (Roche) followed by manufacturing procedures. Various amounts of RNAi were first diluted into RNase free water (Ambion) followed by mixing with 10 ul of Fugene into final 100 ul mixtures. The RNAi mixtures were incubated at room temperature for 10 minutes and then gently added to cell samples. Cells samples were harvested afterward for further analyses.

Cell cycle analyses

For analyzing cell cycle distribution of RNAi or plasmid transfected cells, they were harvested and suspended into 300ul of cold DPBS (Sigma) followed by adding 700ul of 100% cold EtOH dropwise with gently vortexing and incubating in ice for 15 minutes. Subsequently, cell samples were pelleted and resuspended into propidium iodide (PI; Sigma) staining solution (50 ug/ml PI; 0.1 mg/ml RNase A (Sigma); 0.05%

Tritin X-100 in DPBS) for 40 min at 37°C. The stained samples were pelleted by centrifugation and resuspened back into DPBS for analysis using flow cytometer with red fluorescence channel filter.

Cell growth

Viable cell density of High Five cells was measured by using a hemocytometer with trypan blue staining solution to exclude the dead cells.

Semi-quantitative RT-PCR

To determine relative transcription levels, High Five RNA was extracted the concentration was quantified by NanoDrop (Thermo Scientific) and first strand templates of each sample were synthesized from 500 ng of RNA using Superscript RT III (Invitrogen) kit with oligo-dT primers. The first strand cDNA was PCR amplified using CycE primers. Actin primers for PCR amplification were chosen for the internal controls from the RT treatments. The resultant PCR products were checked by 1% agarose gels (Fisher Scientific) and images were taken with a gel imaging camera (AlphaImager HP; Alpha Innotech).

Recombinant his-tagged CycE protein purification and western blotting

To express the histidine-tagged CycE protein, A T25 flask of High Five cells were transfected with pIB-TnCycE vector by Fugene HD (4ug/ml) and cultivated for 4 days before harvested. The cell samples were pelleted and lysated by Cytobuster^{TM} solution (EMD chemicals) in ice for 40 minutes. Subsequently, the cell lysates were purified

using TALON metal affinity resin (Clontech) followed by the instruction. The resultant protein sample was dialyzed overnight in DPBS using dialysis tubing (Spectrum Laboratories). Samples were then run on a 12.5% SDS-PAGE gel and then transferred to nitrocellulose membranes by a BioRad Trans-Blot semi-dry transfer cell. After 5% milk blocking and rinising steps, western blotting was performed to detect the purified CycE using rabbit polyclonal anti-human cyclin E antibody (Rockland immunochemicals) with 1:500 dilution ratio. Secondary antibody incubation was carried out by using the alkaline phosphatase labeled goat anti-rabbit (Sigma) with 1:500 dilution. Color developing step was then performed by using BCIP/NBT solution (Roche).

4.3. Results and Discussion

Identification of T. ni CycE and protein characterization

We used RACE RT-PCR to identify *CycE* sequences. Results indicated that the complete cDNA sequence was 1,518 bp, which would encode a 506 aa protein. We performed both nucleotide and protein BLAST analyses, which revealed significant sequence homology with cyclin E families of different eukaryotics. Figure 4-1a shows the CycE protein sequence alignment between the putative *T. ni* and related species, *Bombyx mori* (silkworm), *Drosophila melanogaster* (fruit fly), and *Aedes aegypti* (mosquito). Sequence homology was significant but not identical, while *B. mori* had 76.75% identity at the amino acid level; *D. melanogaster* and *Aedes aegypti* were less (45.14% and 41.74% respectively).

In addition to sequence validation, we used western blot analyses against human cyclin E to further characterize the *T. ni* CycE at a molecular level. That is, the putative full length CycE was cloned into the insect cell expression vector (pIB/V5-His) yielding plasmid pIB-TnCycE, which was transfected into High-five cells to express a putative histidine-tagged CycE. This protein was purified and probed via rabbit polyclonal anti-human cyclin E. Subsequent band development with Alkaline Phosphatase (AP) labeled goat anti-rabbit IgG and BCIP/NBT signal detection suggested the expressed protein was indeed a CycE (Figure 4-1b). Specifically, controls protein GFPuv yielded no signal (Lane 4). Moreover, the band from the CycE sample was observed between MW 64.2 and 48.8KDa, which match the theoretical MW (61.3 KDa) of the his-tagged, putative CycE. Finally, the band intensity indicated on the western blot increased with a doubling

of loaded sample. Overall, the newly identified gene and protein product appeared by the physical measurements to belong to family of eukaryotic cyclin E.

(a)

```
Trichoplusia_ni                1 -------MAQTGSVCESSEKRLTLKRKRN-----STDDELENMPPLK----------ISP
Bombyx_mori                    1 -------MAESGSPSEASEKRMTLKRKRS-----SSDDELENQPPQK----------IAS
Drosophila_melanogaster        1 MKLEQKRKFIEMDPELGFEPPSAKRQQRLPALYGSEQGNLSSVASSVYTSPVVSVDGQST
Aedes_aegypti                  1 MDLYSSEDASRSSTSEITEPRSRNSRKRK---YTSDDADIENQRPSKRHGGDRRLSPIAA

Trichoplusia_ni               39 VLEEELNDQPAHNVVVESSSCSS---DDEGSQYGAVDQPRS--VYTDLDYNPDSFLSPPS
Bombyx_mori                   39 TLDEQLCDQPALHVVVESSSCSS---DDEGSQYGNSDQPRS--VYTDIDYNPDSFLSPPS
Drosophila_melanogaster       61 QELLSIRSSPAEDLSEAPHSPLPDSPDSPPSPDRGSKQTPVVVRYAAEQVVTSTVVTQKT
Aedes_aegypti                 58 SSAPSVP-IPSVASSAASSNSVP-SINIGSSEYTSDTQSSSDCYSTTADFELYPLVSPPS

Trichoplusia_ni               94 ISD---------------------------------LPNCVLSPLENVARGESTP----
Bombyx_mori                   94 VSD---------------------------------LPNSVLSPLENVARGESTP----
Drosophila_melanogaster      121 EDDDLLDDSCEDYSYDEDDEDDVEEEDDDVEIYSSTISPASSGCSQQQAVNGERTPGLPK
Aedes_aegypti                116 VNSIILSPSCEVSHGSWHTKGDTTPHAN---------RKSSSHSNQQQQRHNENSN---N

Trichoplusia_ni              116 ---HSNKRPSTSKIPCPTLPK-------RKCPLPRLSWADPGDVWNSMCDCDARSSNRKN
Bombyx_mori                  116 ---HSNKRANASKPPCPTPPK-------RKCPLPGLSWADPADVWNSMCECDARSSKKKN
Drosophila_melanogaster      181 HQEQIHHPVSDLMINMRTPMSPAVENGLRQCPLPALAWANAADVWRLMCHRDEQDSRLRS
Aedes_aegypti                164 SSSKSSSNVPPALSCCVTPSS-----DLRSCPLPRFAWADSNQVWKLMCRKDEKASLERE

Trichoplusia_ni              166 PNMFDNHPNLQPRMRAILLDWLNEVCEVYKLHRETFHLTVDYVDRYLSNTEDVQKGRLQL
Bombyx_mori                  166 PNMFDNHPNLQPRMRAILLDWLNEIGTKKTRQMRVRKLTAEGFR-------------SQ
Drosophila_melanogaster      241 ISMLEQHPGLQPRMRAILLDWLIEVCEVYKLHRETFYLAVDYLDRYLHVAHKVQKTHLQL
Aedes_aegypti                219 PNMFDQHPGLQPRMRAILLDWLIEVCEVYKLHRETYYLAVDYIDRFLSRKKEQKKTHLQL

Trichoplusia_ni              226 IGITCLFIAAKVEEVYPPKIGEFAYVTDGACTTDEILLEELLILKILSWSITPITINSWL
Bombyx_mori                  212 VCITCLFIAAKVEEVYPPKIAEFAYVTDGACTTEEILLEELLILKILSWSITPITINSWL
Drosophila_melanogaster      301 IGITCLFVAAKVEEIYPPKIGEFAYVTDGACTERDILNHEKILLQALDWDISPITITGWL
Aedes_aegypti                279 LGITALFVAAKVEEIYPPKIGEFAYVTDGACSEDDILREELLLLSELQWSINPVTVMGWL

Trichoplusia_ni              286 NVYMQLASEGRS---AKRRLLGESDVAAN----ALRSYTFVFPQYSSLEFVICGQLIDLA
Bombyx_mori                  272 NVYMQLASEGKS---AKRRLLGESDVAAN----ALRGYTFVFPQYSSLEFVICGQLVDLA
Drosophila_melanogaster      361 GVYMQLNVNNR-----TPASFSQIGRQKS----AEADDAFIYPQFSGFEFVQTSQLLDLC
Aedes_aegypti                339 GTYMQVNVTSRQMEMMHPHSVGACRKQQTTPSKPQLDESFVYPQFSGMEFAQTAQLIDLC

Trichoplusia_ni              339 VLHVDVNLFAYSAVAAAAIAHAFTKELAIRVSGYNWDVLEPCWRWLAPFASVIRTEGSVC
Bombyx_mori                  325 VLHVDVNLFSYSAVAAAAIAHTYNRELAMRVSGYKWESLSECYTWLEPFARSLREAGAGG
Drosophila_melanogaster      412 TLDVGMANYSYSVLAAAAISHTFSREMALRCSGLDWQVIQPCARWMEPFFRVIS--QKAP
Aedes_aegypti                399 SLDVGLANFPYSVIAAAAVSHTFDRKTATSVSGLDWDAIAPCAKWMEPYFLVICDENEVS

Trichoplusia_ni              399 VVRGGD-GEFLQAAGGLDLICPDVNLDESHRIQSHNVTLDMFDKVYQIMVEQQSV-TQTT
Bombyx_mori                  385 QVRAAD-GEFVQPAAALRHICPDINPDESHRIQQHNVTLDMFDKVYQAILEHS---SQHD
Drosophila_melanogaster      470 YLQLNEQNEQVSNKFGLGLICPNIVTDDSHIIQTHTTTTMDMYDEVLMAQDAAHAMRARIQ
Aedes_aegypti                459 PLALLESNEQVKGSFGLAHVCPNLVSDSSHIIQTHSTSLDMFDRASLRREHLEVVACIIQ

Trichoplusia_ni              457 SEAATSQESEHIYPPTPPASDHKS------------PKTPTTKTPSTRHLSPPPEARRLS
Bombyx_mori                  441 VCPSTSVDTDHIYPPTPPHSDHKS------------PKTPTTKTPSNRHEH----ELRIH
Drosophila_melanogaster      530 ASPATA-LRAPESLLTPPASSHKPDEYLGDEGDETGARSGISSTTTCCNTAASNKGGKSS
Aedes_aegypti                519 QEASPAPLLDPEGLLTPPASSRKS----------LDANNPLEVTNKLVNKT---------

Trichoplusia_ni              505 TE------------
Bombyx_mori                  485 AD------------
Drosophila_melanogaster      589 SNNSVTSCSSRSNP
Aedes_aegypti                     --------------
```

(b)

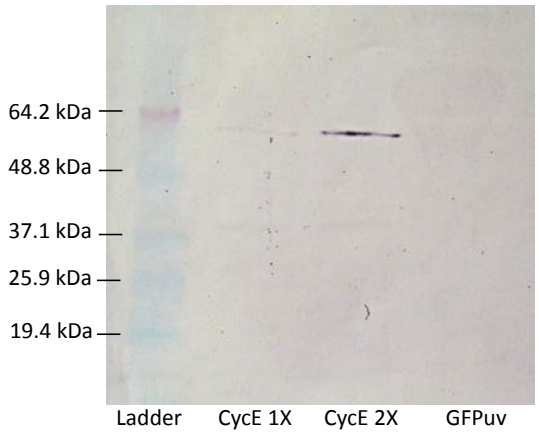

Figure 4-1 Characterization of *T. ni* CycE protein. (a) Protein sequence alignment results between T. ni and its' relatively close species, *Bombyx mori* (silkworm; NCBI

accession # AB457002.2), *Drosophila melanogaster* (fruit fly; NCBI accession # NP_476960) and *Aedes aegypti* (mosquito; NCBI accession # EAT39115.1). The alignment was performed by ClustalW and coloring was performed by BOXSHADE. (b) Western blot results for *T. ni* CycE protein using rabbit anti-cyclin E against human (1:500 dilution). Lane 1: ladder; Lane 2: 5ug CycE; Lane 3: 10ug CycE; Lane 4: 5ug GFP_{uv} (negative control).

Manipulating CycE expression-effects on cell cycle and cell growth

Up-regulation of CycE

In order to confirm the protein is Cyclin E, we examined its function in *T. ni* cells. Specifically, the overexpression of cyclin E in mammalian cells leads to escape from cell cycle regulation and cancerous proliferation. Similar phenomena have been reported in insect *Drosophila* cell cultures and adult flies [141, 142]. This proliferation leads to unchecked progression through G1 to S phase and a decrease of the G1 population. Here, we characterize transcriptional and phenotypic changes of High Five cells associated with elevated CycE expression associated with transfection with pIB-TnCycE.

As shown in Figure 4-2a (Land 4), mRNA transcription level increased significantly at 3 days post- transfection with pIB-TnCycE compared to pIB-EGFP or other controls. In addition, it is also notable that the elevating CycE transcription with pIB-TnCycE treatment enhanced cell proliferation (Figure 4-2b), particularly at 3 days post-transfection. Beyond three days, cell densities were close to the maximum supported by the growth medium. Also as the CycE is expressed from the non-replicating plasmids, the effects on regulating networks would be expected to be transient, particularly in rapid growth environments. Even through the significant enhancement of cell growth, no obvious changes of cell cycle distribution were observed (Figure 4-2c). It is interesting to note that cell cycle distribution for High-Five cells was found to be

heavily skewed towards the G2/M phases (G1:2.5%, S: 6.5%, G2/M: 65%, >4N: ~25%). Not surprisingly, CycE overexpression therefore led to no further distribution shift towards the G2/M phases (Figure 4-2c) even through significant enhancing on cell proliferation was observed. This result lies in contrast to another industrially relevant insect cell line, *Spodoptera frugiperda* (Sf9) which under normal cell culture conditions exhibits 29% of the population in G1 (G1:29%, S: 33%, G2/M: 36%)[143]. In summary, our results indicate that the High-Five cell growth was influenced by *CycE* overexpression.

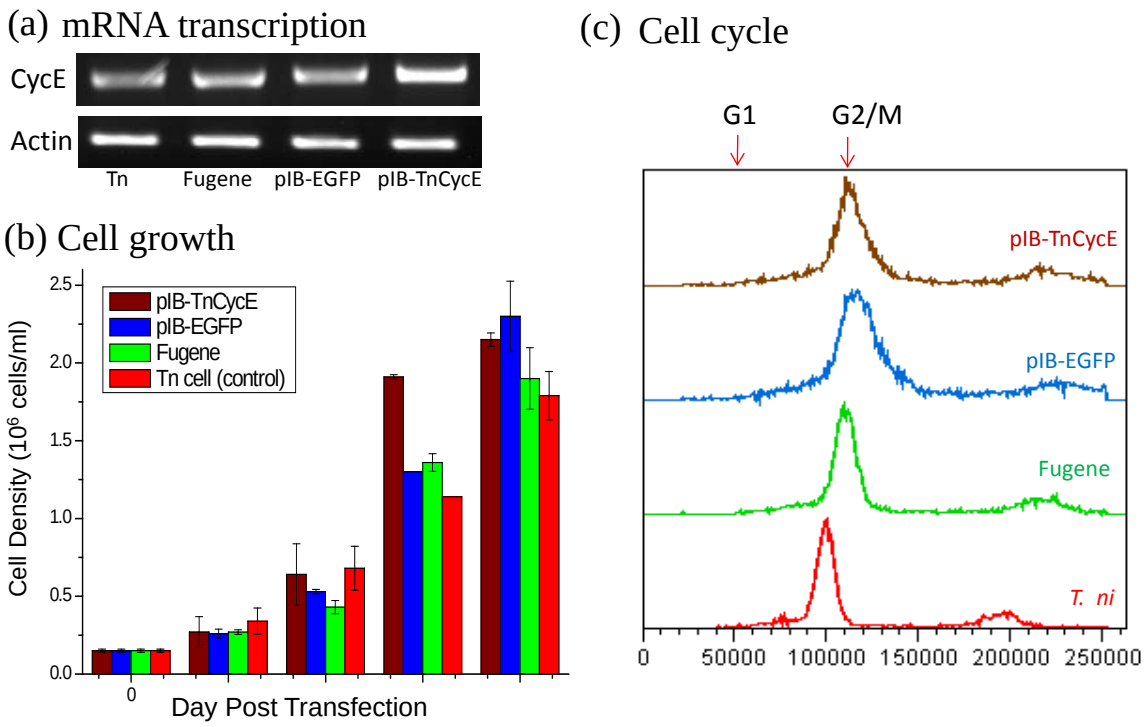

Figure 4-2 Effects of *CycE* up-regulation on cell physiology. Initially 0.2x10^6 cells/ml of suspension High Five cells were treated with Fugene + 4ug/ml pIB-TnCycE vector (for up-regulation), Fugene + 4ug/ml pIB-EGFP vector (control), and Fugene only (control). Cell samples were harvested at 3 day post transfection and subsequently measurement were conducted as followed. (a) mRNA transcriptional level by RT-PCR with actin primers (internal control); (b) time course measurement for cell proliferation was performed by using trypan blue; (c) cell cycle status was determined by flow cytometry using PI staining.

Down-regulation of CycE

In addition to up-regulation, experiments targeting *CycE* down-regulation were conducted. Phenotypic changes to cell cycle phase distribution and cell growth were characterized. To down-regulate CycE, we synthesized dsRNA against T. ni *CycE* using the method by Hebert et al [144]. The selected dsTnCycE sequence as amplified was

~800 bp in length. This relatively long form of dsTnCycE is thought to confer greater stability to dsRNA constructs leading to higher knockdown efficiency of the targeted gene [75]. We then performed studies using High-Five suspension cell cultures transfected with either dsTnCycE or a non-specific dsCAT control. The mRNA level of *CycE* in the experimental population decreased significantly compared to the controls (Figure 4-3a), suggesting dsTnCycE treatment was successful. Cell growth of *CycE* silenced populations was nearly abolished (4ug/ml)(Figure 4-3b). This reduction of growth rate by knockdown was immediately observed only 1 day after transfection and persisted over the entire time course. Analysis of investigating the effect of CycE knockdown on cell cycle phase distribution, we discovered a concentration dependent response to dsTnCycE (Figure 4-3c). That is, peaks at G2/M phases (2N) were significantly shifted into G1 (1N) in a concentration dependent manner, while no shifts were seen for the dsCAT treatment and other controls. Contrasting this to *CycE* upregulation suggests that wild type basal *CycE* abundance in High-Five cells is sufficient for ignoring the G1 to S phase checkpoint. In summary, functional assays which support over-proliferation in the presence of high *CycE* and cell cycle-arrest in low *CycE*, correspond to physical characterization results. That is, the sequence depicted in Figure 1, represents functional full-length *T. ni CycE*.

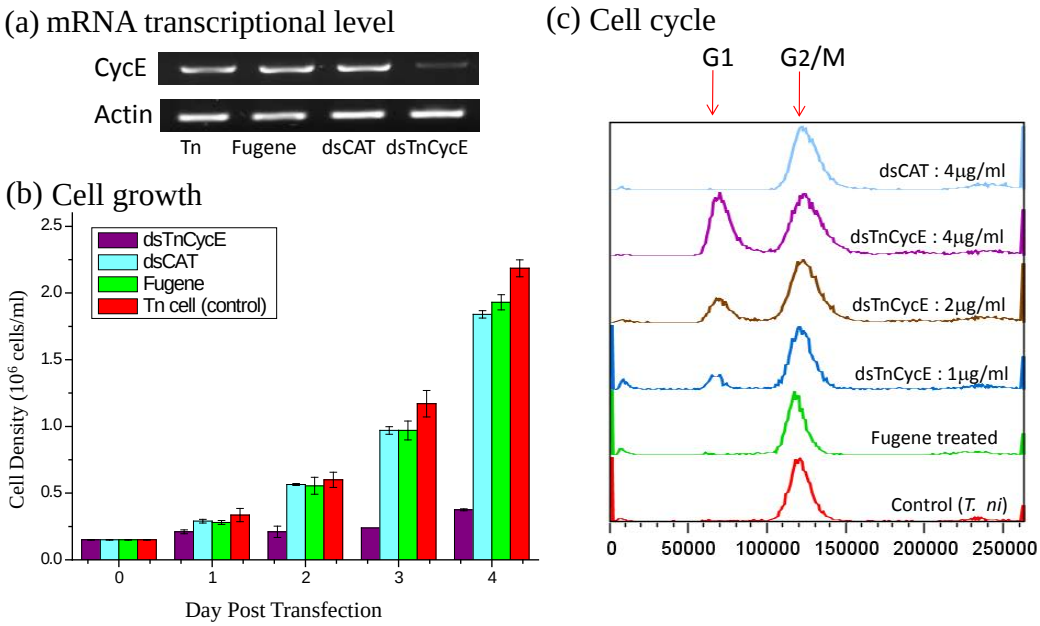

Figure 4-3 Effects of *CycE* down-regulation on cell physiology. Suspension of High Five cells ($0.2x10^6$ cells/ml) were treated with Fugene + 4ug/ml dsTnCycE (for silencing), Fugene + 4ug/ml dsCAT (control), and Fugene only (control). (a) mRNA transcriptional level by RT-PCR with actin primers (internal control) was carried out at 3 day post transfection. (b) Time course measurement for cell proliferation was performed using trypan blue. (c) Dosage-dependent *CycE* silencing on cell cycle shifting was investigated by flow cytometry using PI staining at 3 day post transfection.

Enhancing recombinant protein production-effects of CycE RNAi on baculovirus protein expression

To investigate altering High-Five cell line productivity through cell cycle modulation, we utilized the baculovirus expression system, one of the most popular insect recombinant protein production platforms. Briefly, High-Five cells adhered to 24-well plates were transfected with a broad range of dsTnCycE concentrations for 16 hours, followed by baculovirus (P_{PH}-GFPuv ; GFPuv expression under the polyhedron promoter)

infection with various of MOI(0.1, 1, 10) for 4 days. Subsequently, cells were then harvested and intra-cellular GFPuv expression was analyzed by flow cytometry. The resultant fluorescence intensities were further integrated to determine the overall expression level of GFPuv. As depicted in Figure 4-4, results displayed enhanced GFP expression up to 2.5-fold after treatment with dsTnCycE at high MOI (10). However, at low MOI (0.1 and 1), the effects were not as significant, potentially due to the low expression level of GFPuv. It was also notable that GFP expression peaked at 8 ug/ml dsTnCycE treatment and dropped significantly at 12 ug/ml, potentially indicating the range of dsTnCycE concentration at which cumulative phenotype changes adversely affect overall High-Five cell physiology. Coincidently, similar *CycE* RNAi toxicity was also observed for Drosophila S2 cell line (~9 ug/ml) for optimized recombinant protein productivity [75]. In summary, we demonstrated the use of *CycE* RNAi to enhance baculovirus driven protein expression in adhered High-Five cells.

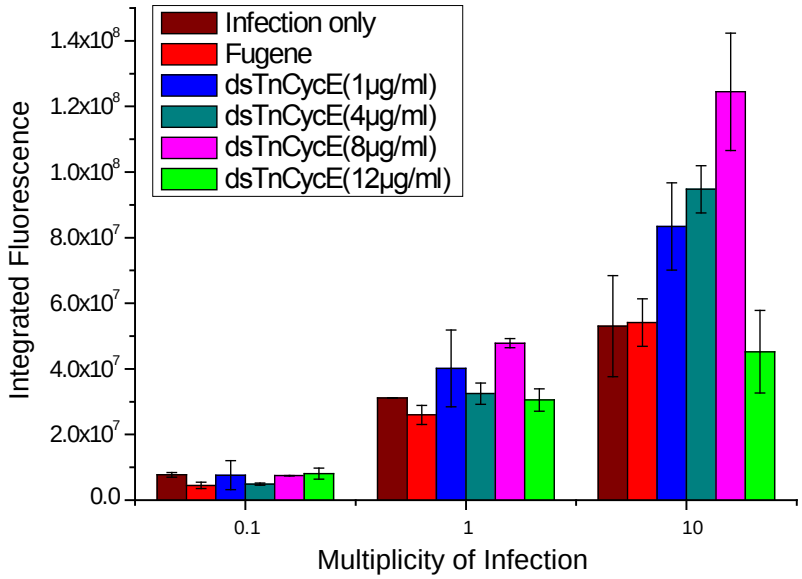

Figure 4-4 Investigation of dosage-dependent dsTnCycE effect on intra-cellular productivity of adhesion High Five cells using baculovirus expression system. Cells were transfected with various concentrations of dsTnCycE (1ug/ml, 4ug/ml, 8ug/ml, and 12ug/ml) using Fugene for 16 hours in prior to infection. Baculovirus AcMNPV that expresses GFP_{uv} under the polyhedron promoter was utilized for infection with different MOI (0.1, 1, and 10). Cell samples were harvested and the fluorescence of intra-cellular GFPuv was measured by flow cytometry for protein productivity at 4 day post infection.

Because High-Five cells efficiently secrete recombinant proteins into culture medium, we also tracked extracellular GFPuv. Briefly, suspension cell cultures were transfected with various concentration of dsCycE for 16 hours, followed by baculovirus infection (MOI=10) for 2 to 7 days. In order to establish the definition between intra-cellular and extra-cellular GFP, 200 µl of each cell culture sample was harvested and centrifuged to separate the supernatant (the extracellular sample) and cell pellet. The cell pellets were then lysed with 200ul CytoBuster ™ lysis buffer, centrifuged to pellet cell debris, and the supernatant harvested to produce the intra-cellular sample. Extracellular and intracellular GFP samples were measured by a plate reader and summed to derive a total product yield. As shown in Figure 4-5a, the intra-cellular GFPuv of control samples

without dsCycE treatment increased significantly by day 3 then dropped thereafter; GFPuv expression of dsTnCycE treated cells, on the contrary, increased steadily over time, reaching a zenith at day 5. Comparing the expression at 4 days post- infection, the dsCycE treated cells was roughly ~ 1.8-fold higher than mock infected cells, confirming the integrated FACS results from Figure 4-4. Measurements of extra-cellular GFPuv (Figure 4-5b), however, showed a converse outcome where supernatants from control wells had higher GFPuv than treatment wells. Apparently, the dsRNA reduced the secretion rate of GFPuv in transfected cells. Yet, the overall production of GFPuv (Figure 4-5c) derived by combining intra-cellular and extra-cellular RFU values, resulted in a nearly 1.5-fold increase.

In summary, a cell cycle arrest strategy using dsTnCycE successfully enhanced the cell productivity. We speculate two potential reasons. First, as mentioned above, dsRNA treatment prolonged the GFPuv production window to 5^{th} day post-infection. This is atypical of baculovirus production where the peak productivity normally appears in 2 to 4 days. Second, the secretion of GFPuv into the medium was reduced, which might indicate the baculovirus lytic process from the host was suppressed. This observation is partially supported by Braunagel et al., (1998) [143] who showed that sf9 cells pre-arrested in G1 and S phases prior to baculovirus infection do not affect viral DNA replication, but that progeny virus assembly and maturation, e.g. occlusion-derived virus, become abnormal. Further investigations would be necessary to resolve the mechanism behind this phenomenon.

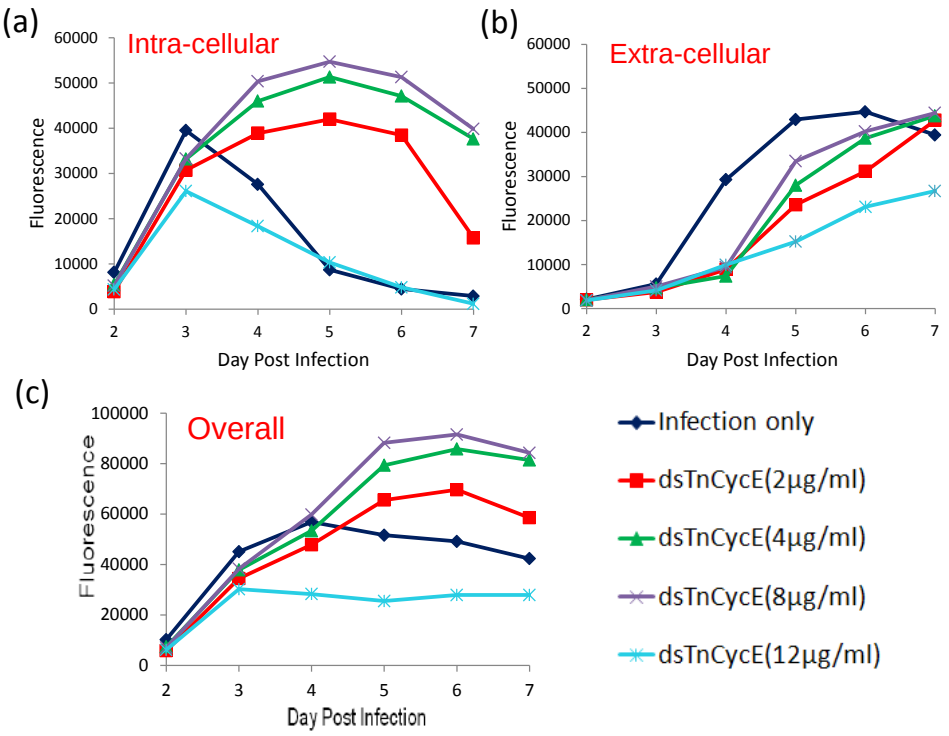

Figure 4-5 Effects of dosage-dependent dsTnCycE on intra- and extra-cellular productivity of suspension High Five cells using baculovirus expression system. Cells were transfected with various concentrations of dsTnCycE (2ug/ml, 4ug/ml, 8ug/ml, and 12ug/ml) using Fugene for 16 hours in prior to infection. Same baculovirus which produces GFP_{uv} was utilized for infection with MOI 10. For preparing samples, cells for extra-cellular GFP_{uv} were prepared by collecting the supernatant form the infected cell medium; the cell pellets from the infected cell medium was lysed by cytobuster lysis buffer and the supernatant was collected as the intra-cellular GFP_{uv}. Both intra- and extra-cellular GFP_{uv} intensities were measured by a plate reader from 2 to 7 day post infection and represented in (a) and (b) respectively. Overall productivity, as shown in (c), was calculated by the summation of the intra- and extra-celluar GFP_{uv} intensities.

4.4. Conclusions

We have successfully identified the complete cyclin E cDNA sequence of *T. ni* and characterized the recombinant *CycE* through physical and functional analyses. We

have observed that the up-regulation of *CycE* actively facilitated cell growth without perturbing the cell cycle distribution; meanwhile, down-regulation of *CycE* expression through *in vitro* dsTnCycE caused cell cycle arrest at G1 phase and inhibited cell growth significantly. Finally, we demonstrated the concentration-dependent dsTnCycE silencing effect on enhancing both the intra- and extra-cellular GFPuv production of *T. ni* cell culture via the baculovirus expression system. An optimal concentration of RNAi for protein productivity was identified.

The RNAi strategy for cell cycle regulation, unlike some procedures using chemicals, is biological based and metabolizable for cells, which might add further benefit by extending cell longevity and productivity. This approach which targets a global condition using a simple molecular-based switch holds great promise to enhance yield particularly if genome engineering approaches in eukaryotic cells can't be achieved.

Chapter 5. Summary

5.1. Assembling of antibodies and antigens through protein G biofabrication

In Chapter 2, we engineered protein G, an IgG binding domain, with an enzyme-activatable pentatyrosine "pro-tag" that allows covalent coupling to the pH stimuli-responsive biopolymer, chitosan, which is spatially addressed through electro-signaling. Different configurations or formats, such as multiwell plates, micropatterned electrodes, and fiber networks are demonstrated. We assembled both HG3T and antibodies, finding assembly in a linear fashion so that quantitative assessment of antibodies and antigens became feasible. This biofabrication approach provides bottom-up hierarchical assembly of functional supramolecular structures that could be designed to facilitate integration into devices.

5.2. Developing a smart bacterial switch device with targeting, sensing, and switching capabilities

We engineered an *E. coli* K-12 W3110 with a genetic circuit that endows it with targeting, sensing and switching capabilities. The protein G is displayed on the outer membrane of the bacteria which allows for flexible targeting through antibody-antigen interaction. In addition, we created a cell-based biological switch that was activated based on surface receptor density on mammalian cells. That is, we found that the accumulation of bacteria at the target surface triggered a "switch" in response to EGFR density on a mammalian cell model. This serves as a phenotype focusing system as it

maintains the switch in an “off” state until the desired threshold is reached. We believe this switch could potentially be exploited via synthetic biology tool for the synthesis and delivery of human therapeutics.

5.3. Exploiting RNAi to control cell cycle/cell growth of eukaryotic insect cell for enhancing recombinant protein productivity

We employed a metabolic engineering approach to “tune” the cell cycle to overcome checkpoint processes. This facilitated faster cell growth and depending on the added concentration, arrested cells at a high productivity phase for recombinant protein synthesis. To do this, we identified the complete *cyclin E* (*CycE*) sequence from industrially relevant, *Trichoplusia ni* genomes (cDNA). We then then synthesized *T. ni CycE* specific RNAi to test *CycE* suppression. By knocking down (through RNAi) and overexpressing *CycE* (on an expression plasmid) gene expression, we successfully lowered and raised cell growth, respectively. We also investigated the dose-dependent effects of dsCycE on recombinant protein production using the baculovirus expression system. We found by downregulating *CycE*, we enhanced protein (GFPuv) synthesis by 1.5-fold.

5.4. Future directions

5.4.1. Incorporating of invasin protein into the QS switch for bacteria targeting and invasion

We demonstrated that we could create bacteria that would recognize EGFR receptor densities on the surface of cancer cell lines. Upon reaching a threshold density, the cells produced DsRed. It would be quite interesting to have the cells produce a peptide on the outer surface to facilitate its direct attachment to the cell surface and subsequent cargo delivery. We have hypothesized that invasin [145] could provide this function. Grillot-Courvalin et al. (1998) [145] showed Inter-kingdom gene transfer from *E. coli* K12 bacteria to mammalian cells by using invasin, an invasion promoting protein derived from *Yersinia pseudotuberculosis* that triggers endocytosis. Many follow-up gene therapy applications utilizing the same bacteria carrier have been reported [146-148]. This invasin delivery approach is powerful in terms of delivery efficiency; but lacks targeting specificity. We therefore seek to combine specific targeting (through antibody) and cargo delivery (through invasin triggered endocytosis) based upon the bacteria switch we have created. Specifically, we could replace the DsRed model protein with invasin in our genetic circuitry, which would allow the bacteria to decide whether or not to invade the mammalian cell on which they have docked based on the targeting density. We envision this new invasin switch would be beneficial in some therapeutic cases by providing a means of tightly controllable, high threshold, low background response *in vitro* or *in vivo*.

5.4.2. Using RNAi as a cell proliferation control agent in bacteria cancer therapeutics

Using an RNAi approach, we have demonstrated the competence of cell cycle regulation in order to block aberrant cell growth arising from skewed cell cycle phase distributions. RNAi based cancer therapies are already under development [149-151]. Xiang et al. (2006) [152] demonstrated the feasibility of using bacteria to synthesize and carry short hairpin RNA to perform gene silencing in mammalian cell and mice systems. Here, we would seek to exploit bacteria as a targeted vector to deliver RNAi to knockdown cell cycle genes for cancer therapy.

Chapter 6. Bibliography

1. Tigges, M. and M. Fussenegger, *Recent advances in mammalian synthetic biology-design of synthetic transgene control networks.* Curr Opin Biotechnol, 2009. **20**(4): p. 449-60.
2. Andrianantoandro, E., et al., *Synthetic biology: new engineering rules for an emerging discipline.* Mol Syst Biol, 2006. **2**: p. 2006 0028.
3. Nandagopal, N. and M.B. Elowitz, *Synthetic biology: integrated gene circuits.* Science, 2011. **333**(6047): p. 1244-8.
4. Khalil, A.S. and J.J. Collins, *Synthetic biology: applications come of age.* Nat Rev Genet, 2010. **11**(5): p. 367-79.
5. Fritz, B.R., et al., *Biology by design: from top to bottom and back.* J Biomed Biotechnol, 2010. **2010**: p. 232016.
6. Atsumi, S., T. Hanai, and J.C. Liao, *Non-fermentative pathways for synthesis of branched-chain higher alcohols as biofuels.* Nature, 2008. **451**(7174): p. 86-9.
7. Nam, Y.S., et al., *Biologically templated photocatalytic nanostructures for sustained light-driven water oxidation.* Nat Nanotechnol, 2010. **5**(5): p. 340-4.
8. Dueber, J.E., et al., *Synthetic protein scaffolds provide modular control over metabolic flux.* Nat Biotechnol, 2009. **27**(8): p. 753-9.
9. Moon, T.S., et al., *Use of modular, synthetic scaffolds for improved production of glucaric acid in engineered E. coli.* Metab Eng, 2010. **12**(3): p. 298-305.
10. Danino, T., et al., *A synchronized quorum of genetic clocks.* Nature, 2010. **463**(7279): p. 326-30.
11. Tigges, M., et al., *A tunable synthetic mammalian oscillator.* Nature, 2009. **457**(7227): p. 309-12.
12. Fung, E., et al., *A synthetic gene-metabolic oscillator.* Nature, 2005. **435**(7038): p. 118-22.
13. Howorka, S., *Rationally engineering natural protein assemblies in nanobiotechnology.* Curr Opin Biotechnol, 2011. **22**(4): p. 485-91.
14. Marchisio, M.A. and F. Rudolf, *Synthetic biosensing systems.* Int J Biochem Cell Biol, 2011. **43**(3): p. 310-9.
15. Lu, T.K., A.S. Khalil, and J.J. Collins, *Next-generation synthetic gene networks.* Nat Biotechnol, 2009. **27**(12): p. 1139-50.
16. Papapostolou, D. and S. Howorka, *Engineering and exploiting protein assemblies in synthetic biology.* Mol Biosyst, 2009. **5**(7): p. 723-32.
17. Gitzinger, M., et al., *Controlling transgene expression in subcutaneous implants using a skin lotion containing the apple metabolite phloretin.* Proc Natl Acad Sci U S A, 2009. **106**(26): p. 10638-43.
18. Ruder, W.C., T. Lu, and J.J. Collins, *Synthetic biology moving into the clinic.* Science, 2011. **333**(6047): p. 1248-52.
19. Chen, Y.Y. and C.D. Smolke, *From DNA to targeted therapeutics: bringing synthetic biology to the clinic.* Sci Transl Med, 2011. **3**(106): p. 106ps42.
20. Weber, W. and M. Fussenegger, *Emerging biomedical applications of synthetic biology.* Nat Rev Genet, 2011.
21. Shankar, S. and M.R. Pillai, *Translating cancer research by synthetic biology.* Mol Biosyst, 2011. **7**(6): p. 1802-10.

22. Sia, S.K., B.M. Gillette, and G.J. Yang, *Synthetic tissue biology: tissue engineering meets synthetic biology.* Birth Defects Res C Embryo Today, 2007. **81**(4): p. 354-61.
23. Kindsmuller, K. and R. Wagner, *Synthetic biology: impact on the design of innovative vaccines.* Hum Vaccin, 2011. **7**(6): p. 658-62.
24. Burbelo, P.D., et al., *Synthetic biology for translational research.* Am J Transl Res, 2010. **2**(4): p. 381-9.
25. Schmidt, F.R., *Recombinant expression systems in the pharmaceutical industry.* Appl Microbiol Biotechnol, 2004. **65**(4): p. 363-72.
26. Kamionka, M., *Engineering of therapeutic proteins production in Escherichia coli.* Curr Pharm Biotechnol, 2011. **12**(2): p. 268-74.
27. Terpe, K., *Overview of bacterial expression systems for heterologous protein production: from molecular and biochemical fundamentals to commercial systems.* Appl Microbiol Biotechnol, 2006. **72**(2): p. 211-22.
28. Duan, F. and J.C. March, *Engineered bacterial communication prevents Vibrio cholerae virulence in an infant mouse model.* Proc Natl Acad Sci U S A, 2010. **107**(25): p. 11260-4.
29. Saeidi, N., et al., *Engineering microbes to sense and eradicate Pseudomonas aeruginosa, a human pathogen.* Mol Syst Biol, 2011. **7**: p. 521.
30. Yu, H., *Bacteria-mediated disease therapy.* Appl Microbiol Biotechnol, 2011. **92**(6): p. 1107-13.
31. Oelschlaeger, T.A., *Bacteria as tumor therapeutics?* Bioeng Bugs, 2010. **1**(2): p. 146-7.
32. Pawelek, J.M., K.B. Low, and D. Bermudes, *Tumor-targeted Salmonella as a novel anticancer vector.* Cancer Res, 1997. **57**(20): p. 4537-44.
33. Yu, Y.A., et al., *Visualization of tumors and metastases in live animals with bacteria and vaccinia virus encoding light-emitting proteins.* Nat Biotechnol, 2004. **22**(3): p. 313-20.
34. Fox, M.E., et al., *Anaerobic bacteria as a delivery system for cancer gene therapy: in vitro activation of 5-fluorocytosine by genetically engineered clostridia.* Gene Ther, 1996. **3**(2): p. 173-8.
35. Patyar, S., et al., *Bacteria in cancer therapy: a novel experimental strategy.* J Biomed Sci, 2010. **17**(1): p. 21.
36. St Jean, A.T., M. Zhang, and N.S. Forbes, *Bacterial therapies: completing the cancer treatment toolbox.* Curr Opin Biotechnol, 2008. **19**(5): p. 511-7.
37. Mengesha, A., et al., *Potential and limitations of bacterial-mediated cancer therapy.* Front Biosci, 2007. **12**: p. 3880-91.
38. Stritzker, J., et al., *Tumor-specific colonization, tissue distribution, and gene induction by probiotic Escherichia coli Nissle 1917 in live mice.* Int J Med Microbiol, 2007. **297**(3): p. 151-62.
39. Forbes, N.S., *Profile of a bacterial tumor killer.* Nat Biotechnol, 2006. **24**(12): p. 1484-5.
40. Wei, M.Q., et al., *Facultative or obligate anaerobic bacteria have the potential for multimodality therapy of solid tumours.* Eur J Cancer, 2007. **43**(3): p. 490-6.
41. Forbes, N.S., *Engineering the perfect (bacterial) cancer therapy.* Nat Rev Cancer, 2010. **10**(11): p. 785-94.

42. Liu, Y., et al., *Biofabrication to build the biology-device interface.* Biofabrication, 2010. **2**(2): p. 022002.
43. Mironov, V., et al., *Biofabrication: a 21st century manufacturing paradigm.* Biofabrication, 2009. **1**(2): p. 022001.
44. Wu, L.Q. and G.F. Payne, *Biofabrication: using biological materials and biocatalysts to construct nanostructured assemblies.* Trends in Biotechnology, 2004. **22**(11): p. 593-599.
45. Wu, P., D.G. Castner, and D.W. Grainger, *Diagnostic devices as biomaterials: a review of nucleic acid and protein microarray surface performance issues.* J Biomater Sci Polym Ed, 2008. **19**(6): p. 725-53.
46. Yi, H., et al., *Biofabrication with chitosan.* Biomacromolecules, 2005. **6**(6): p. 2881-94.
47. Tanaka, G., et al., *Fabrication of an antibody microwell array with self-adhering antibody binding protein.* Anal Biochem, 2006. **350**(2): p. 298-303.
48. Rusmini, F., Z. Zhong, and J. Feijen, *Protein immobilization strategies for protein biochips.* Biomacromolecules, 2007. **8**(6): p. 1775-89.
49. March, J.C. and W.E. Bentley, *Quorum sensing and bacterial cross-talk in biotechnology.* Curr Opin Biotechnol, 2004. **15**(5): p. 495-502.
50. Hooshangi, S. and W.E. Bentley, *From unicellular properties to multicellular behavior: bacteria quorum sensing circuitry and applications.* Curr Opin Biotechnol, 2008. **19**(6): p. 550-5.
51. Roy, V., B.L. Adams, and W.E. Bentley, *Developing next generation antimicrobials by intercepting AI-2 mediated quorum sensing.* Enzyme Microb Technol, 2011. **49**(2): p. 113-23.
52. Steindler, L. and V. Venturi, *Detection of quorum-sensing N-acyl homoserine lactone signal molecules by bacterial biosensors.* FEMS Microbiol Lett, 2007. **266**(1): p. 1-9.
53. Tsao, C.Y., et al., *LuxS coexpression enhances yields of recombinant proteins in Escherichia coli in part through posttranscriptional control of GroEL.* Appl Environ Microbiol, 2011. **77**(6): p. 2141-52.
54. Tsao, C.Y., et al., *Autonomous induction of recombinant proteins by minimally rewiring native quorum sensing regulon of E. coli.* Metab Eng, 2010. **12**(3): p. 291-7.
55. Tessema, M., U. Lehmann, and H. Kreipe, *Cell cycle and no end.* Virchows Arch, 2004. **444**(4): p. 313-23.
56. Molinari, M., *Cell cycle checkpoints and their inactivation in human cancer.* Cell Prolif, 2000. **33**: p. 261–274.
57. Coffman, J.A., *Cell cycle development.* Dev Cell, 2004. **6**(3): p. 321-7.
58. van den Heuvel, S., *Cell cycle regulation*2005: WormBook.
59. Murray, A.W., *Recycling the cell cycle: cyclins revisited.* Cell, 2004. **116**(2): p. 221-34.
60. Vermeulen, K., D.R. Van Bockstaele, and Z.N. Berneman, *The cell cycle: a review of regulation, deregulation and therapeutic targets in cancer.* Cell Prolif, 2003. **36**(3): p. 131-49.
61. Sclafani, R.A. and T.M. Holzen, *Cell cycle regulation of DNA replication.* Annu Rev Genet, 2007. **41**: p. 237-80.

62. Tachibana, K.E., M.A. Gonzalez, and N. Coleman, *Cell-cycle-dependent regulation of DNA replication and its relevance to cancer pathology.* J Pathol, 2005. **205**(2): p. 123-9.
63. Wurm, F.M., *Production of recombinant protein therapeutics in cultivated mammalian cells.* Nat Biotechnol, 2004. **22**(11): p. 1393-8.
64. Elledge, S.J., *Cell cycle checkpoints: preventing an identity crisis.* Science, 1996. **274**(5293): p. 1664-72.
65. Guo, S. and K.J. Kemphues, *par-1, a gene required for establishing polarity in C. elegans embryos, encodes a putative Ser/Thr kinase that is asymmetrically distributed.* Cell, 1995. **81**(4): p. 611-20.
66. Fire, A., et al., *Potent and specific genetic interference by double-stranded RNA in Caenorhabditis elegans.* Nature, 1998. **391**(6669): p. 806-11.
67. Li, C.X., et al., *Delivery of RNA interference.* Cell Cycle, 2006. **5**(18): p. 2103-9.
68. Tong, A.W., Y.A. Zhang, and J. Nemunaitis, *Small interfering RNA for experimental cancer therapy.* Curr Opin Mol Ther, 2005. **7**(2): p. 114-24.
69. Cullen, L.M. and G.M. Arndt, *Genome-wide screening for gene function using RNAi in mammalian cells.* Immunol Cell Biol, 2005. **83**(3): p. 217-23.
70. Kamath, R.S. and J. Ahringer, *Genome-wide RNAi screening in Caenorhabditis elegans.* Methods, 2003. **30**(4): p. 313-21.
71. Boutros, M., et al., *Genome-wide RNAi analysis of growth and viability in Drosophila cells.* Science, 2004. **303**(5659): p. 832-5.
72. Kramera, S.F. and W.E. Bentley, *RNA interference as a metabolic engineering tool: potential for in vivo control of protein expression in an insect larval model.* Metabolic Engineering 2003. **5**: p. 183-190.
73. Timmons, L. and A. Fire, *Specific interference by ingested dsRNA.* Nature, 1998. **395**: p. 854.
74. Dykxhoorn, D.M., C.D. Novina, and P.A. Sharp, *Killing the Messenger: Short RNAs that Silence Gene Expression.* Nature Reviews, 2003. **4**: p. 457-467.
75. March, J.C. and W.E. Bentley, *RNAi-based tuning of cell cycling in Drosophila S2 cells--effects on recombinant protein yield.* Appl Microbiol Biotechnol, 2007. **73**(5): p. 1128-35.
76. Kingsmore, S.F., *Multiplexed protein measurement: technologies and applications of protein and antibody arrays.* Nat Rev Drug Discov, 2006. **5**(4): p. 310-20.
77. Haab, B.B., *Applications of antibody array platforms.* Curr Opin Biotechnol, 2006. **17**(4): p. 415-21.
78. Pavlickova, P., E.M. Schneider, and H. Hug, *Advances in recombinant antibody microarrays.* Clinica Chimica Acta, 2004. **343**(1-2): p. 17-35.
79. Nordon, R.E. and S. Craig, *Hollow-fibre affinity cell separation.* Adv Biochem Eng Biotechnol, 2007. **106**: p. 129-50.
80. Fang, X. and W.W. Zhang, *Affinity separation and enrichment methods in proteomic analysis.* J Proteomics, 2008. **71**(3): p. 284-303.
81. Hansen, K.M. and T. Thundat, *Microcantilever biosensors.* Methods, 2005. **37**(1): p. 57-64.

82. Fowler, J.M., M.C. Stuart, and D.K.Y. Wong, *Self-assembled layer of thiolated protein G as an immunosensor scaffold.* Analytical Chemistry, 2007. **79**(1): p. 350-354.
83. Schmid, A.H., et al., *Site-directed antibody immobilization on gold substrate for surface plasmon resonance sensors.* Sensors and Actuators B-Chemical, 2006. **113**(1): p. 297-303.
84. Bange, A., H.B. Halsall, and W.R. Heineman, *Microfluidic immunosensor systems.* Biosens Bioelectron, 2005. **20**(12): p. 2488-503.
85. Yager, P., et al., *Microfluidic diagnostic technologies for global public health.* Nature, 2006. **442**(7101): p. 412-418.
86. Herr, A.E., et al., *Microfluidic immunoassays as rapid saliva-based clinical diagnostics.* Proceedings of the National Academy of Sciences of the United States of America, 2007. **104**(13): p. 5268-5273.
87. Jiang, X., et al., *Immunosensors for detection of pesticide residues.* Biosens Bioelectron, 2008. **23**(11): p. 1577-87.
88. Akerstrom, B., et al., *Protein G: a powerful tool for binding and detection of monoclonal and polyclonal antibodies.* J Immunol, 1985. **135**(4): p. 2589-92.
89. Vijayendran, R.A. and D.E. Leckband, *A quantitative assessment of heterogeneity for surface-immobilized proteins.* Anal Chem, 2001. **73**(3): p. 471-80.
90. Lee, J.M., et al., *Direct immobilization of protein G variants with various numbers of cysteine residues on a gold surface.* Analytical Chemistry, 2007. **79**(7): p. 2680-2687.
91. Chen, T.H., et al., *Nature-inspired creation of protein-polysaccharide conjugate and its subsequent assembly onto a patterned surface.* Langmuir, 2003. **19**(22): p. 9382-9386.
92. Lewandowski, A.T., et al., *Tyrosine-based "activatable pro-tag": enzyme-catalyzed protein capture and release.* Biotechnol Bioeng, 2006. **93**(6): p. 1207-15.
93. Chen, T., et al., *In vitro protein-polysaccharide conjugation: tyrosinase-catalyzed conjugation of gelatin and chitosan.* Biopolymers, 2002. **64**(6): p. 292-302.
94. Ahmed, S.R., A.T. Lutes, and T.A. Barbari, *Specific capture of target proteins by oriented antibodies bound to tyrosinase-immobilized Protein A on a polyallylamine affinity membrane surface.* Journal of Membrane Science, 2006. **282**(1-2): p. 311-321.
95. Freddi, G., et al., *Tyrosinase-catalyzed modification of Bombyx mori silk fibroin: Grafting of chitosan under heterogeneous reaction conditions.* Journal of Biotechnology, 2006. **125**(2): p. 281-294.
96. Anghileri, A., et al., *Tyrosinase-catalyzed grafting of sericin peptides onto chitosan and production of protein-polysaccharide bioconjugates.* Journal of Biotechnology, 2007. **127**(3): p. 508-519.
97. Payne, G.F. and S.R. Raghavan, *Chitosan: a soft interconnect for hierarchical assembly of nano-scale components.* Soft Matter, 2007. **3**(5): p. 521-527.
98. Gao, D., et al., *Fabrication of antibody arrays using thermally responsive elastin fusion proteins.* J Am Chem Soc, 2006. **128**(3): p. 676-7.
99. Shi, X.W., et al., *Chitosan fibers: versatile platform for nickel-mediated protein assembly.* Biomacromolecules, 2008. **9**(5): p. 1417-23.

100. Cha, H.J., et al., *Observations of green fluorescent protein as a fusion partner in genetically engineered Escherichia coli: Monitoring protein expression and solubility.* Biotechnology and Bioengineering, 2000. **67**(5): p. 565-574.
101. Payne, G.F., M.V. Chaubal, and T.A. Barbari, *Enzyme-catalysed polymer modification : reaction of phenolic compounds with chitosan films.* Polymer, 1996. **37**(20): p. 4643-4648.
102. Horspool, W.M., P.I. Smith, and J.M. Tedder, *Chemistry of ortho Benzoquinones 4. Addition of Primary Aromatic Amines to 1,2-Benzoquinone.* J. Chem. Soc. (C). 1971. **1**: p. 138-140.
103. Hempen, C., et al., *Liquid chromatographic/mass spectrometric investigation on the reaction products in the peroxidase-catalyzed oxidation of o-phenylenediamine by hydrogen peroxide.* Anal Bioanal Chem, 2005. **382**(1): p. 234-8.
104. Lewandowski, A.T., et al., *Protein assembly onto patterned microfabricated devices through enzymatic activation of fusion pro-tag.* Biotechnol Bioeng, 2008. **99**(3): p. 499-507.
105. Luo, X., et al., *Programmable assembly of a metabolic pathway enzyme in a pre-packaged reusable bioMEMS device.* Lab Chip, 2008. **8**(3): p. 420-30.
106. Yu, M., J. Hwang, and T.J. Deming, *Role of L-3,4-dihydroxyphenylalanine in mussel adhesive proteins.* J. Am. Chem. Soc., 1999. **121**: p. 5825-26.
107. Wu, L.Q., et al., *Voltage-dependent assembly of the polysaccharide chitosan onto an electrode surface.* Langmuir, 2002. **18**(22): p. 8620-8625.
108. Fernandes, R., et al., *Electrochemically induced deposition of a polysaccharide hydrogel onto a patterned surface.* Langmuir, 2003. **19**(10): p. 4058-4062.
109. Wu, L.Q., et al., *Spatially selective deposition of a reactive polysaccharide layer onto a patterned template.* Langmuir, 2003. **19**(3): p. 519-524.
110. Fernandes, R., et al., *Thermo-biolithography: a technique for patterning nucleic acids and proteins.* Langmuir, 2004. **20**(3): p. 906-13.
111. Schiffman, J.D. and C.L. Schauer, *Cross-linking chitosan nanofibers.* Biomacromolecules, 2007. **8**(2): p. 594-601.
112. Qin, Y.M., et al., *Preparation and characterization of silver containing chitosan fibers.* Journal of Applied Polymer Science, 2007. **104**(6): p. 3622-3627.
113. Rathke, T.D. and S.M. Hudson, *Review of Chitin and Chitosan as Fiber and Film Formers.* Journal of Macromolecular Science-Reviews in Macromolecular Chemistry and Physics, 1994. **C34**(3): p. 375-437.
114. Christodoulides, N., et al., *Application of microchip assay system for the measurement of C-reactive protein in human saliva.* Lab Chip, 2005. **5**(3): p. 261-9.
115. Koev, S.T., et al., *Mechano-transduction of DNA hybridization and dopamine oxidation through electrodeposited chitosan network.* Lab on a Chip, 2007. **7**(1): p. 103-111.
116. Park, J.J., et al., *Chitosan-mediated in situ biomolecule assembly in completely packaged microfluidic devices.* Lab Chip, 2006. **6**(10): p. 1315-21.
117. Waters, C.M. and B.L. Bassler, *Quorum sensing: cell-to-cell communication in bacteria.* Annu Rev Cell Dev Biol, 2005. **21**: p. 319-46.

118. Miller, M.B. and B.L. Bassler, *Quorum sensing in bacteria.* Annu Rev Microbiol, 2001. **55**: p. 165-99.
119. Surette, M.G. and B.L. Bassler, *Quorum sensing in Escherichia coli and Salmonella typhimurium.* Proc Natl Acad Sci U S A, 1998. **95**(12): p. 7046-50.
120. Jayaraman, A. and T.K. Wood, *Bacterial quorum sensing: signals, circuits, and implications for biofilms and disease.* Annu Rev Biomed Eng, 2008. **10**: p. 145-67.
121. Fernandes, R., et al., *Engineered biological nanofactories trigger quorum sensing response in targeted bacteria.* Nat Nanotechnol, 2010. **5**(3): p. 213-7.
122. Datsenko, K.A. and B.L. Wanner, *One-step inactivation of chromosomal genes in Escherichia coli K-12 using PCR products.* Proceedings of the National Academy of Sciences of the United States of America, 2000. **97**(12): p. 6640-6645.
123. Francisco, J.A., C.F. Earhart, and G. Georgiou, *Transport and anchoring of beta-lactamase to the external surface of Escherichia coli.* Proc Natl Acad Sci U S A, 1992. **89**(7): p. 2713-7.
124. Fisher, A.C., et al., *Production of secretory and extracellular N-linked glycoproteins in Escherichia coli.* Appl Environ Microbiol, 2011. **77**(3): p. 871-81.
125. Warner, J.R., et al., *Rapid profiling of a microbial genome using mixtures of barcoded oligonucleotides.* Nat Biotechnol, 2010. **28**(8): p. 856-62.
126. Xu, X., et al., *The genomic sequence of the Chinese hamster ovary (CHO)-K1 cell line.* Nat Biotechnol, 2011. **29**(8): p. 735-41.
127. Harper, J.V. and G. Brooks, *The mammalian cell cycle: an overview.* Methods Mol Biol, 2005. **296**: p. 113-53.
128. Slavov, N. and D. Botstein, *Coupling among growth rate response, metabolic cycle, and cell division cycle in yeast.* Mol Biol Cell, 2011. **22**(12): p. 1997-2009.
129. Boye, E. and K. Nordstrom, *Coupling the cell cycle to cell growth.* EMBO Rep, 2003. **4**(8): p. 757-60.
130. Tapon, N., K.H. Moberg, and I.K. Hariharan, *The coupling of cell growth to the cell cycle.* Curr Opin Cell Biol, 2001. **13**(6): p. 731-7.
131. Kumar, N., P. Gammell, and M. Clynes, *Proliferation control strategies to improve productivity and survival during CHO based production culture.* Cytotechnology, 2007. **53**: p. 33–46.
132. Gali-Muhtasib, H. and N. Bakkar, *Modulating cell cycle: current applications and prospects for future drug development.* Curr Cancer Drug Targets, 2002. **2**(4): p. 309-36.
133. Stein, G.S. and A.B. Pardee, *Cell Cycle and Growth Control* Second Edition ed2005: John Wiley & Sons, Inc.
134. Fussenegger, M., et al., *Controlled proliferation by multigene metabolic engineering enhances the productivity of Chinese hamster ovary cells.* Nat Biotechnol, 1998. **16**(5): p. 468-72.
135. Watanabe, S., J. Shuttleworth, and M. Al-Rubeai, *Regulation of cell cycle and productivity in NS0 cells by the over-expression of p21CIP1.* Biotechnol Bioeng, 2002. **77**(1): p. 1-7.
136. van den Heuvel, S., *The C. elegans cell cycle: overview of molecules and mechanisms.* Methods Mol Biol, 2005. **296**: p. 51-67.
137. Iba, H., A. Fukuda, and Y. Okada, *Rate of major protein synthesis during the cell cycle of Caulobacter crescentus.* J Bacteriol, 1978. **135**(2): p. 647-55.

138. Mazur, X., et al., *Higher productivity of growth-arrested Chinese hamster ovary cells expressing the cyclin-dependent kinase inhibitor p27.* Biotechnol Prog, 1998. **14**(5): p. 705-13.
139. Bi, J.X., J. Shuttleworth, and M. Al-Rubeai, *Uncoupling of cell growth and proliferation results in enhancement of productivity in p21CIP1-arrested CHO cells.* Biotechnol Bioeng, 2004. **85**(7): p. 741-9.
140. Cha, H.J., et al., *Insect larval expression process is optimized by generating fusions with green fluorescent protein.* Biotechnol Bioeng, 1999. **65**(3): p. 316-24.
141. Lai, Z.C., et al., *Control of cell proliferation and apoptosis by mob as tumor suppressor, mats.* Cell, 2005. **120**(5): p. 675-85.
142. Jia, J., et al., *The Drosophila Ste20 family kinase dMST functions as a tumor suppressor by restricting cell proliferation and promoting apoptosis.* Genes Dev, 2003. **17**(20): p. 2514-9.
143. Braunagel, S.C., et al., *Autographa californica nucleopolyhedrovirus infection results in Sf9 cell cycle arrest at G2/M phase.* Virology, 1998. **244**(1): p. 195-211.
144. Hebert, C.G., J.J. Valdes, and W.E. Bentley, *Investigating apoptosis: characterization and analysis of Trichoplusia ni-caspase-1 through overexpression and RNAi mediated silencing.* Insect Biochem Mol Biol, 2009. **39**(2): p. 113-24.
145. Grillot-Courvalin, C., et al., *Functional gene transfer from intracellular bacteria to mammalian cells.* Nat Biotechnol, 1998. **16**(9): p. 862-6.
146. Anderson, J.C., et al., *Environmentally controlled invasion of cancer cells by engineered bacteria.* J Mol Biol, 2006. **355**(4): p. 619-27.
147. Castagliuolo, I., et al., *Engineered E. coli delivers therapeutic genes to the colonic mucosa.* Gene Ther, 2005. **12**(13): p. 1070-8.
148. Simon, B.E. and J.A. Leong, *Gene transfer to fish cells by attenuated invasive Escherichia coli.* Mar Biotechnol (NY), 2002. **4**(3): p. 303-9.
149. Pai, S.I., et al., *Prospects of RNA interference therapy for cancer.* Gene Ther, 2006. **13**(6): p. 464-77.
150. Abdelrahim, M., et al., *RNAi and cancer: Implications and applications.* J RNAi Gene Silencing, 2006. **2**(1): p. 136-45.
151. Phalon, C., D.D. Rao, and J. Nemunaitis, *Potential use of RNA interference in cancer therapy.* Expert Rev Mol Med, 2010. **12**: p. e26.
152. Xiang, S., J. Fruehauf, and C.J. Li, *Short hairpin RNA-expressing bacteria elicit RNA interference in mammals.* Nat Biotechnol, 2006. **24**(6): p. 697-702.